รายงานวิจัยฉบับสมบูรณ์

โครงการ การพัฒนาอุปกรณ์ตรวจวัดบนกระดาษสำหรับวิเคราะห์ออคซาเลต

โดย ผศ.ดร. วิจิตรา เดือนฉาย

เมษายน 2562

สัญญาเลขที่ MRG6080171

รายงานวิจัยฉบับสมบูรณ์

โครงการ การพัฒนาอุปกรณ์ตรวจวัดบนกระดาษสำหรับวิเคราะห์ออคซาเลต

ผู้วิจัย
ผศ.ดร. วิจิตรา เดือนฉาย
ภาควิชาเคมี คณะวิทยาศาสตร์ มหาวิทยาลัยเทคโนโลยีพระจอมเกล้าธนบุรี

สนับสนุนโดยสำนักงานคณะกรรมการการอุดมศึกษา สำนักงานกองทุนสนับสนุนการวิจัย
และมหาวิทยาลัยเทคโนโลยีพระจอมเกล้าธนบุรี
(ความเห็นในรายงานนี้เป็นของผู้วิจัย สกอ. และ สกว. ไม่จำเป็นต้องเห็นด้วยเสมอไป)

Contents

บทคัดย่อ

รหัสโครงการ : MRG6080171

ชื่อโครงการ : การพัฒนาอุปกรณ์ตรวจวัดบนกระดาษสำหรับวิเคราะห์ออคซาเลต

ชื่อนักวิจัย : ผศ.ดร. วิจิตรา เดือนฉาย

อีเมลล์ : wijitar_29@hotmail.com

ระยะเวลาโครงการ : 2 ปี ระหว่างวันที่ 4 เมษายน 2560 ถึงวันที่ 4 เมษายน 2562

บทคัดย่อ:
ร่างกายมนุษย์ที่มีสุขภาพปกติ จะมีปริมาณออคซาเลตในปัสสาวะ 20 มิลลิกรัมต่อปัสสาวะ 24 ชั่วโมง ถ้าปัสสาวะมีระดับออคซาเลตมากเกิน จะทำให้เกิดการรวมตัวกันระหว่างแคลเซียมกับออคซาเลต กลายเป็นก้อนนิ่วในไต ดังนั้นการตรวจปริมาณออคซาเลตในปัสสาวะจึงมีความจำเป็นต่อการเฝ้าระวัง และติดตามโรคนิ่วในไต อุปกรณ์ตรวจวัดบนกระดาษได้รับความสนใจจากนักวิทยาศาสตร์เป็นอย่างมาก เนื่องจากราคาวัสดุและกระบวนการสร้างอุปกรณ์ไม่แพง ในงานนี้พัฒนาอุปกรณ์ตรวจวัดกระดาษเพื่อตรวจวัดออคซาเลตด้วยสังเกตการเปลี่ยนแปลงสีของปฏิกิริยาเคมี งานวิจัยนี้สามารถวิเคราะห์เชิงปริมาณได้ตั้งแต่ระดับความเข้มข้นตั้งแต่ 10 ถึง 1000 ไมโครโมลต่อลิตร ด้วยสมการเส้นตรงระหว่างตัวแปรต้นคือความเข้มข้นของออคซาเลตในหน่วย ไมโครโมลต่อลิตร และตัวแปรตามคือ ความเข้มของสีวัดด้วยโปรแกรม ImageJ ได้สมการดังนี้ $y = 0.0086x + 34.978$ มีค่าสัมพันธ์เชิงเส้น (R^2) เท่ากับ 0.9994 ค่าความเข้มข้นต่ำสุดที่วัดได้ด้วยตาเปล่าเท่ากับ 10 ไมโครโมลต่อลิตร จากการทดสอบเติมออคซาเลตลงในปัสสาวะสังเคราะห์ได้ร้อยละการคืนกลับเท่ากับ 81-92 ดังนั้นอุปกรณ์ตรวจวัดบนกระดาษนี้สามารถใช้วิเคราะห์ออคซาเลตในตัวอย่างจริงได้อย่างรวดเร็วและมีความว่องไวในการตรวจวัดเหมาะที่จะประยุกต์ใช้กับผู้ป่วยนอกสถานที่ได้

คำหลัก: ออคซาเลต; การตรวจวัดเชิงสี; อุปกรณ์ตรวจวัดบนกระดาษ

Abstract

Project Code : MRG6080171

Project Title : Development of paper-based devices for oxalate determination

Investigator : Assist. Dr. Wijitar Dungchai

E-mail Address : Wijitar_29@hotmail.com

Project Period : 2 years during 4th April 2016 to 4th April 2018

Abstract:

Human bodies are normally excrete oxalate in urine, which is 20 mg / urine 24hr. If your oxalate levels are too high, the oxalate can combine with calcium to form calcium oxalate cause kidney stone. In addition, analysis of oxalate concentration have been extensively studied from a health perspective: their relationship to kidney stone formation and their relationship to calcium absorption and metabolism. Paper-based devices have attracted significant attention because of the ultra-low cost of the materials and manufacturing processes used. Here, we will develop the paper-based devices coupled with colorimetric detection for the determination of oxalate. The quantitative detection of oxalate ranged from 10 – 1000 μM, with a linear equation, y = 0.0086x + 34.978, and a correlation coefficient (R^2) = 0.9994. The detection limit was 10 μM by the naked eye. The recoveries of oxalate spiked in artificial urine samples evaluated by our cPADs were in the range of 81 – 92%. This simple cPAD for rapid and sensitive oxalate determination should be useful for diagnostic urinary oxalate measurements for point-of-care monitoring.

Keywords : Food Oxalate; Colorimetric Detection; Paper-based Device

Executive Summary

วัตถุประสงค์

1. เพื่อออกแบบชุดตรวจวัดบนกระดาษ เพื่อการตรวจวัดออคซาเลต
2. ประยุกต์วิธีการการวิเคราะห์ที่ได้รับการพัฒนาแล้วสำหรับใช้หาปริมาณของออคซาเลตในตัวอย่างจริง

การดำเนินงานวิจัย และผลงานวิจัยที่ได้รับอย่างย่อ ๆ

1. ค้นคว้าข้อมูลและเอกสารที่เกี่ยวข้อง
2. ได้รูปแบบอุปกรณ์ที่เหมาะสมสำหรับการตรวจวัดออคซาเลตด้วยตาเปล่า
3. ศึกษาภาวะที่เหมาะสมสำหรับการตรวจวัดออคซาเลต
4. ศึกษาค่าตัวแปรที่สำคัญทางการวิเคราะห์ ได้แก่ ค่าความเข้มข้นต่ำสุดของการวิเคราะห์ ช่วงความสัมพันธ์ของสัญญาณและความเข้มข้น ความสามารถในการทำซ้ำได้
5. นำภาวะที่เหมาะสมที่ได้จากการศึกษาในสารตัวอย่างปัสสาวะจริง
6. สรุปผลการทดลอง และเขียน manuscript เพื่อตีพิมพ์ในวารสารระดับนานาชาติ
7. ผลลงานได้รับการตีพิมพ์ในวารสารระดับนานาชาติ ชื่อวารสาร Analytical Science (impact factor = 1.355) ดังเอกสารแนบ
8. พัฒนาชุดอุปกรณ์ตรวจวัดคลอไรด์ และผลงานได้รับการตอบรับให้ตีพิมพ์ในวารสาร Analyst (impact factor = 3.864) ดังเอกสารแนบ

CHAPTER I
INTRODUCTION

The prevalence and incidence of kidney stones is reported to be increasing across the world. There is historical evidence of the influence of diet on stone formation. The first documented increase in stone disease occurred during the 16th century when European Stein-Schneiders (stone cutters) found that their services were more in demand. During this period, there were improvements in food production and corn became a popular food staple. The increased consumption of starchy foods derived from corn promoted obesity, currently a known risk factor for stone formation. Other dietary risk factors for stone formation have been identified. There is strong evidence that diminished fluid and calcium consumption are risk factors. Increased oxalate consumption has also been demonstrated to promote stone formation. Epidemiologic studies have demonstrated that increased sodium and animal protein intake have an equivocal impact on stone risk. Global climate change is another environmental factor that affects stone disease rates. There are reported about the association between increased environmental temperatures and increased kidney stone rates [1]. In Thailand, kidney stone disease is a longstanding medical illness and still a common public health problem. Piyaratana Tosukhowong reported about Kidney Stone: Current Status in the Northeast of Thailand. Increased Incidence of urolithiasis IPD (nephrolithiasis, Renal stone, Kidney stone) was reported [2]. The report of The Ministry of Health in Thai found that statistics of the incidence of kidney stones in the urinary tract of the patient increased from 99.25 per 100,000 of the population in 2007 to 122.46 in 2010. Most of the population in the Northeast provinces was found to have the highest prevalence of up to 16.9%. Most stones found in the age range 40-50 years and common in males than females up to 2 times, and found a recurrence within 2 years after the surgery, up to 39% [3-4].

The chemical composition of the majority of stones is calcium oxalate (70%) being the rest calcium phosphate (hydroxyapatite or brushite), magnesium and ammonium phosphate (struvite), uric acid and cystine principally. Oxalic acid ($C_2H_2O_4$) is found in common food. When consumed food that have oxalic acid into the body, it will be integrated with other minerals occurred as crystals of oxalate such as calcium oxalate, sodium oxalate, magnesium oxalate and potassium oxalate [5]. When this occurs, the compounds formed are

usually referred to as oxalate salts. Oxalate is a metabolic end product when gets it in human body have normal range is 10-30 mg/24h in urine [6]; and 0.8-2.50 μmol/L in plasma [7]. Determination of oxalate is particularly useful in food chemistry and in clinical analysis is importance for diagnosis and medical management. Most oxalate is a waste product made by the body and has no function in humans. This level of oxalate in urine and plasma are leads to formation of calcium oxalate kidney stones [8-9].

Kidney stones caused by calcium oxalate are a major constituent of more than two thirds of renal stones which are likely to increase both in the region and all over the world. The kidney stones can cause renal function deteriorates and the cause of kidney failure, end-stage renal disease. The occurrence of kidney stones has many causes and risk factors that contribute to gallstones. As well as some vegetables or foods that contain oxalate cause kidney stones. In addition, kidney stones, gallstones over a very high incidence. Both patients and governments have lost the cost of treatment is very significant. The amount of oxalic acid can get each day without the risk about 22 grams for a person weighing 60 kilograms, or about 378 mg/kg body weight [5]. Therefore, finding a method to measure the accurate, efficient, convenient, fast and affordable is important to help patients or the general public aware of the risk of gallstones and can be prevented before they become severe.

In this work, we proposed to develop an inexpensive, simple and rapid distance-based colorimetric detection for the detection of oxalate using paper-based device.

References

1. Romero, V.; Akpinar, H.M.D.; Dean, G.M.D.; Assimos, M.D. “Kidney Stones: A Global Picture of Prevalence, Incidence, and Associated Risk Factors” Reviews in urology, 2010; 12 ; e86-e96.

2. Piyaratana Tosukhowong “Kidney Stone: Current Status in the Northeast of Thailand.” Conference of sunpasit hospital, 8 January 2015 , online: http://www.sunpasit.go.th/booking/index.php?files=viewdocs&room_id=1

3. Yanagawa, M.; Kawamura, J.; Onishi, T.; Soga, N.; Kameda, K.; Sriboonlue, P. “Incidence of urolithiasis in northeast Thailand” Int J Urol, 1997; 4; 537-40.

4. Chanapa, P. “The Risk Factors of Kidney Stones Focusing on Calcium and Oxalate” Songkla Med J, 2011; 29; 299-308.

5. Chongchaithet, N. “Knowledge oxalate” USDA Agricultured Research Service, 2006

6. Pundir, C.S.; Thakur, M.; Satypal, “Determination of urinary oxalate with Cl- and NO3- insensitive oxalate oxidase purified from sorghum leaves” Clinil Chem, 1998; 44; 1364-1365.

7. Pundir, C.S.; Kuchhal, N.K.; Thakur, M.; Satypal, “Determination of plasma oxalate with chloride ion insensitive oxalate oxidase” Ind J Biochem Biophys, 1998; 35; 120-122.

8. Hogkinson, A. “Oxalic acid in biology and medicine” Academic press, New york, 1977; 104-158.

9. Robertson, W.G.; Hughes, H. “Importance of mild hyperoxaluria in the pathogenesis of urolithiasis-new evidence from studies in the Arabian peninsula” Scanning Microsc, 1993, 7, 391-401.

CHAPTER II

Experimental

PART A OXALATE DETERINATION

2.1 Chemicals and materials

All chemicals used in the experiment are analytical reagent (AR) grade. Creatinine, formate dehydrogenase, 3-(4,5-dimethylthiazol-2yl)-2,5-diphenyltetrazolium bromide (MTT), nicotinamide adenine dinucleotide (NAD^+), oxalate decarboxylase, 1-methoxy-5-methylphenazinium methyl sulfate (PMS), urea [$Co(NH_2)_2$] were obtained from Sigma-Aldrich (St. Louis, MO). Monobasic sodium phosphate ($NaHPO_4 \cdot 2H_2O$), dibasic sodium phosphate ($Na_2HPO_4 \cdot 2H_2O$), magnesium sulfate ($MgSO_4 \cdot 7H_2O$), sodium hydrogen phosphate ($NaHPO_4 \cdot 2H_2O$) and sodium dihydrogen phosphate ($NaH_2PO_4 \cdot 7H_2O$) were bought from Panreac (Barcelona, Spain). Ammonium chloride (NH_4Cl), calcium chloride ($CaCl_2 \cdot 2H_2O$), citric acid ($C_6H_8O_7 \cdot H_2O$), potassium chloride (KCl), sodium chloride (NaCl), sodium oxalate ($Na_2C_2O_4$), tri-sodium citrate ($Na_3C_6H_5 \cdot 2H_2O$) and uric acid were bought from Fisher Scientific (Pittsburgh, PA). Sodium hydrogen carbonate ($NaHCO_3$) was purchased from Merck (Darmstadt, Germany). Whatman No.1 filter paper was bought from Cole-Parmer (Vernon Hills, IL). All glassware was thoroughly cleaned with freshly prepared 3:1 HCl/HNO_3 and rinsed with Milli-Q water prior to use. NAD^+ was dissolved in phosphate buffer pH 7.4 whereas Sodium oxalate ($Na_2C_2O_4$) was prepared using citrate-phosphate buffer pH 5.0. Milli-Q water from Millipore ($R \geq 18.2\ M\Omega\ cm^{-1}$) was used throughout these experiments.

2.2 Instrumentation

The results of colorimetric detection were recorded with scanner (Scx-3405, Samsung) using 600-dpi resolution and the color of whole spot was analyzed by Image J program (RGB color mode)

2.3 Preparation of paper-based colorimetric device (cPAD)

The pattern of cPAD was created in Corel Draw designs (Fig. 1) and these devices were transferred to the wax printing (ColorQube, Xerox, Thailand) using Whatman No.1. Then they were baked at 110 $^{\circ}C$ in an oven for 5 minutes. The back side of cPADs was attached with adhesive tape.

2.4 Study of optimal conditions

Prior to the determination of artificial urinary oxalate samples, the optimal conditions: various concentrations of 1-methoxy-5-methylphenazinium methyl sulfate (PMS) at 1, 3 and 5 mM, 3-(4,5-dimethylthiazol-4-yl)-2,5-diphenyl tetrazolium bromide (MTT) at 0.1, 0.3, 0.4 and 0.5 M, and nicotinamide adenine dinucleotide (NAD^+) at 5, 10, 25, 40 and 57 mM, as well as various analysis time at 5, 15, 30 and 45 minutes were investigated. The step of dropped the reactants on the center of cPAD, one microliter of each reagent was sequentially dropped following by 3 units/mL oxalate decarboxylase, 40 mM of NAD^+, 50 units/mL formate dehydrogenase, and MTT and we then let it dried prior to dropping in the next each reagent. During optimal condition, five microliters of 200 μM oxalate mixed with PMS (ratio 4:1) were spotted on loading zone. The sample/standard solutions were incubated for 30 minutes at the room temperature. After incubation that PADs were recorded with scanner (Scx-3405, Samsung) using 600-dpi resolution and then the intensity of color were analyzed with Image J program (RGB color mode) using the whole spot (3 mm.). The intensity difference was calculated by the purple color intensity generating from sample/standard oxalate solution subtracted with background color intensity.

2.5 Analytical Performance

The linear relationship of oxalate were investigated using the optimized conditions and the oxalate standard concentration range of 0-1000 μmol/L. According to our assay relating with formate pathway (Fig. 1), the formate concentration in the range of 0-1000 μmol/L were also studied to verify in term of formate interference. Precision of our cPAD was then investigated using replicated the detection of 200 and 400 μM oxalate (n=10) under the optimized conditions

2.6 Applications

To evaluate the accuracy and utility of our proposed cPAD, oxalate in artificial urine samples were quantified by our cPADs. The artificial urine sample without oxalate was prepared by the method of Chutipongtanate and Thongboonkerd which contained 0.44 g of $CaCl_2 \cdot 2H_2O$, 0.45 g of creatinine, 2.25 g of KCl, 0.50 g of $MgSO_4 \cdot 7H_2O$, 1.48 g of $Na_3C_6H_5 \cdot 2H_2O$, 3.17 g of NaCl, 0.17 g of $NaHCO_3$, 0.05 g of $NaHPO_4 \cdot 7H_2O$, 0.05 g of $NaH_2PO_4 \cdot 2H_2O$, 1.29 g of Na_2SO_4, 0.80 g of NH_4Cl, 12.13 g of urea and 0.17 g of uric acid in 1000.00 mL of deionized water (Solution A). Artificial urine samples of healthy people (200 μM oxalate, S1-S2) were prepared by weighing 0.026x g of $Na_2C_2O_4$ whereas artificial urine

samples of unhealthy people (400 μM oxalate, S3-S4) were prepared by weighing 0.053x g of $Na_2C_2O_4$. All samples were adjusted the volume with solution A to final volume 1000.00 mL. Prior to analysis, spiked samples were dilute 5 times with citrate-phosphate buffer pH 5.0 for adjusting the pH of sample. Each sample was replicated analysis for 3 times (n=3).

PART B: Distance–based Paper Sensor for Determination of Chloride ion Using Silver Nanoparticles

2.1 Chemicals and Materials

Silver nanoparticles (1,000 mg L^{-1}) with diameter of 10 nm were obtained from the Sensor Research Unit at Department of Chemistry, Chulalongkorn University, Thailand. Standard solutions of cations (Cr^{3+}, Mn^{2+}, Cd^{2+}, Cu^{2+}, Zn^{2+} and Fe^{3+} in

2% HNO_3 and Hg^{2+} in 12% HNO_3) were purchased from Sigma-Aldrich (AA grade). Standard anions (NaCl, $NaHCO_3$, $NaNO_3$, $NaNO_2$, NaF, KI, KBr, NaH_2PO_4 and $MgSO_4$) were purchased from Merck, Germany. All chemicals used in experiment were analytical reagent (AR grade) and solutions were prepared using high pure water from Mill-Q

(R ≥18 MΩ cm). Whatman No.1 filter paper was bought from Cole-Parmer (VernonHills, IL).

2.2 Instrumentation

UV–visible absorption spectra were recorded with a UV-visible spectrometer (Lambda 35, Perkin15 Elmer Instruments, USA) using quartz cuvettes (1.0 cm path length) for characterizing silver nanoparticles (AgNPs). The shapes and particle sizes were determined using a Transmission Electron Microscope (TEM, JEOL, JEM-2010) and Scanning Electron Microscope (SEM, JEOL, JSM-6610 LV).

2.3 Preparation of the silver nanoparticles

Silver nanoparticles (AgNPs) solution was prepared according to the previously reported method.[41] Briefly, a solution of silver nitrate ($AgNO_3$) and reducing agent was prepared by dissolving in starch solution. After that, the $AgNO_3$ solution was added to reducing agent solution at a flow rate of 2 mL s^{-1} under vigorous stirring at room

temperature. The colorless solution became dark yellow, indicating the formation of the small silver nanoparticles. After stirring for 30 min, the synthesized AgNPs were boiled for 2 h and cooled down to room temperature for 12 h. The shape and particle size distributions of AgNPs were confirmed with UV–visible spectroscopy, Scanning Electron Microscopy (SEM) and Transmission Electron Microscopy (TEM). The absorbance spectra were recorded using a UV-Visible spectrophotometer in the wavelength range of 350-600 nm.

2.4 Device fabrication and operation

Briefly, the pattern of the device was designed in the shape of a thermometer using CorelDraw and consisted of a sample inlet (diameter 7 mm) and a straight channel for detection zone with a width 3.5 mm and length of channel 40 mm. The designed width of the hydrophobic wax was 3 pt. The design was printed on Whatman No.1 filter paper using a wax printer (Xerox ColorQube 8870, Japan). After printing, the device was placed in an oven for 2 min at 150 °C and then cooled to room temperature. The back side of the device was sealed with tape to prevent solution leakage through the device. The AgNPs were spotted onto the detection channel using a pipette and allowed to dry. After that,

20 µL of standard or sample solution mixed with H_2O_2 was added to the sample zone, where it was carried by capillary action along the flow channel and reacted with AgNPs along the detection channel.

2.5 Optimization of distance-based devices

To optimize the distance-based devices, the effect of reaction times and pH (pH range 3 to 10) were evaluated. For this study, 250 mg L^{-1} of Cl^- was used to obtain optimal conditions for Cl^- detection because of the maximum allowable Cl^- level by the World Health Organization (WHO) for drinking water and natural water at 250 mg L^{-1}. The optimum ratios of chloride and hydrogen peroxide (Cl^-:H_2O_2) were studied by using ratio of 250 mg L^{-1} Cl^- and 0.04% (v/v) H_2O_2 at 1:1, 2:1 and 3:1 by v/v.

2.6 Applications for real samples

The mineral water samples were purchased from a local supermarket. One part was analyzed by Ion chromatography (Dionex Integrion HPIC, Thermo-Fisher Scientific Inc. USA). For the second part, water samples were mixed with 0.04% (v/v) of H_2O_2 to the sample (ratio 1:1 v/v) prior to analysis with our device immediately.

CHAPTER III

Results and Discussion

PART A: OXALATE DETERINATION

3.1 Determination of oxalate

The previous enzymatic system used in the colorimetric oxalate detection was reported two systems; oxalate oxidase and oxalate decarboxylase. In the presence of oxalate, oxalate oxidase will produce hydrogen peroxide whereas oxalate decarboxylase will produce formate and carbon dioxide. Oxalate decarboxylase degraded oxalic acid faster than oxalate oxidase [31]. Furthermore, oxalate decarboxylase was not as sensitive to chlorate and chlorite as oxalate oxidase. Up to 4 mM chlorate ions in the previous reported, the highest concentration tested, had no inhibitory effect on oxalate decarboxylase whereas had effect on oxalate oxidase activity. Thus we have chosen the oxalate decarboxylase enzymatic system on cPAD as showed in Fig. 1A. The concentration of enzyme was used in 3 units/mL oxalate decarboxylase and 50 units/mL formate dehydrogenase that were higher than in solution test. However, the cost per test is still lower than a solution test according to using microliter level of enzyme on our cPAD.

The MTT assay is normally applied for a colorimetric assay for assessing cell metabolic activity. NAD(P)H-dependent cellular oxidoreductase enzymes may, under defined conditions, reflect the number of viable cells present. These enzymes are capable of reducing the tetrazolium dye MTT 3-(4,5-dimethylthiazol-2-yl)-2,5-diphenyltetrazolium bromide to its insoluble formazan, which has a purple color. The insoluble purple formazan has been selected for our cPAD because the insoluble compound can reduce the distribution of non-equally flow into the edge of loading zones. Moreover, the yellow color changing to purple color in the presence of oxalate is easy to distingue by naked eye. In the next sections, the optimization of PMS, MTT and NAD+ concentration was studied.

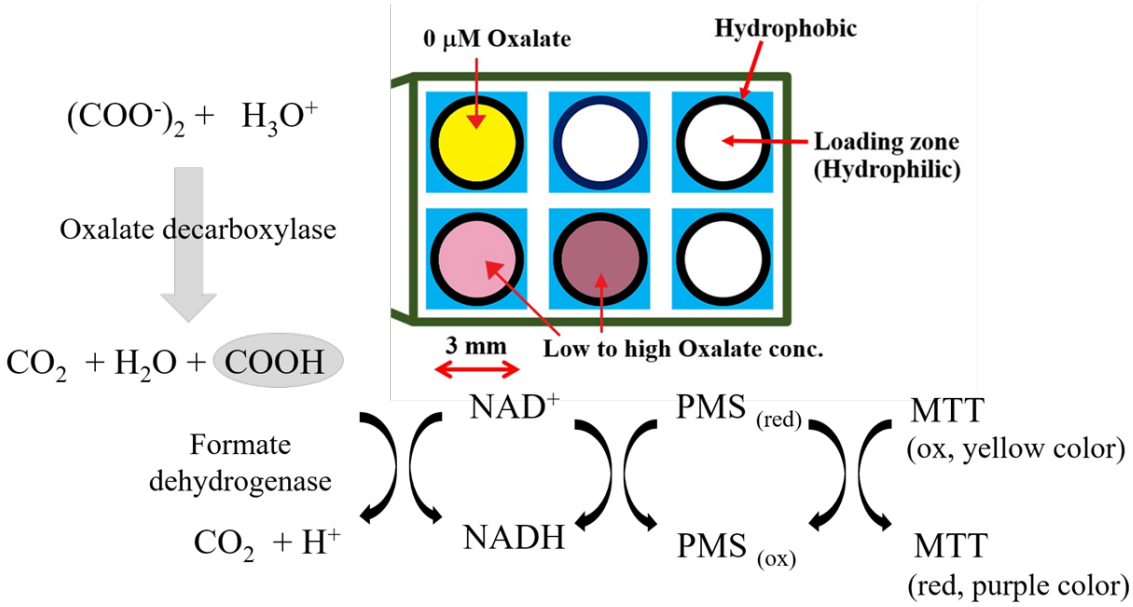

Figure 1A Pattern of cPAD for determination of oxalate

3.1.1 Effect of PMS, MTT and NAD+ concentration

The concentration of PMS, MTT and NAD+ has directly effect on the purple color intensity thus we have optimized PMS concentration in the range of 1, 3, and 5 mM which the saturated PMS solution was found over 5 mM. An increase intensity difference was observed as PMS concentration was increased from 1 to 3 mM as result shown in Fig. 2A. The intensity difference was not significantly different between 3 and 5 mM PMS so we selected 3 mM as the optimized PMS concentration.

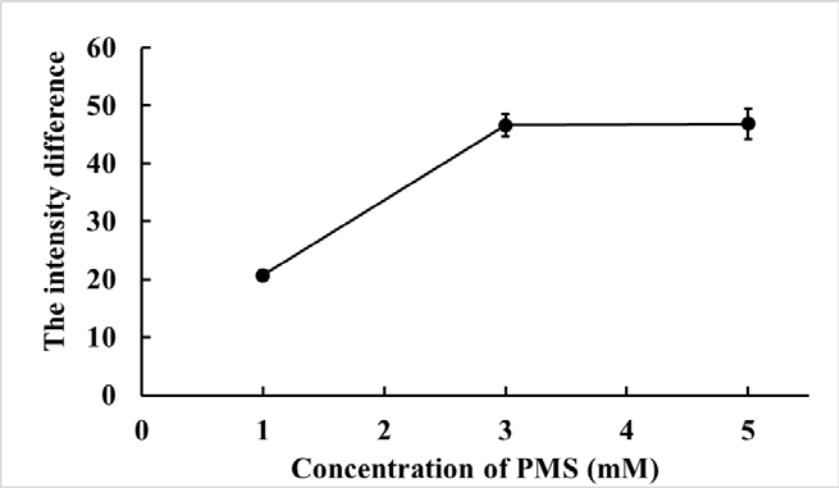

Figure 2A Optimization of PMS concentration at 0.3 M MTT, 57 mM NAD+, and 200 μM oxalate. The color intensity was recorded at 30 min analysis time.

The optimal MTT concentration was also investigated in the ranging 0.1 to 0.5 M. When MTT concentration was increased from 0.1 to 0.3 M, the intensity difference dramatically increased but the intensity difference retained constant after 0.3 M MTT as showed in Fig. 3A. Thus we chose MTT concentration at 0.3 M for the further experimental.

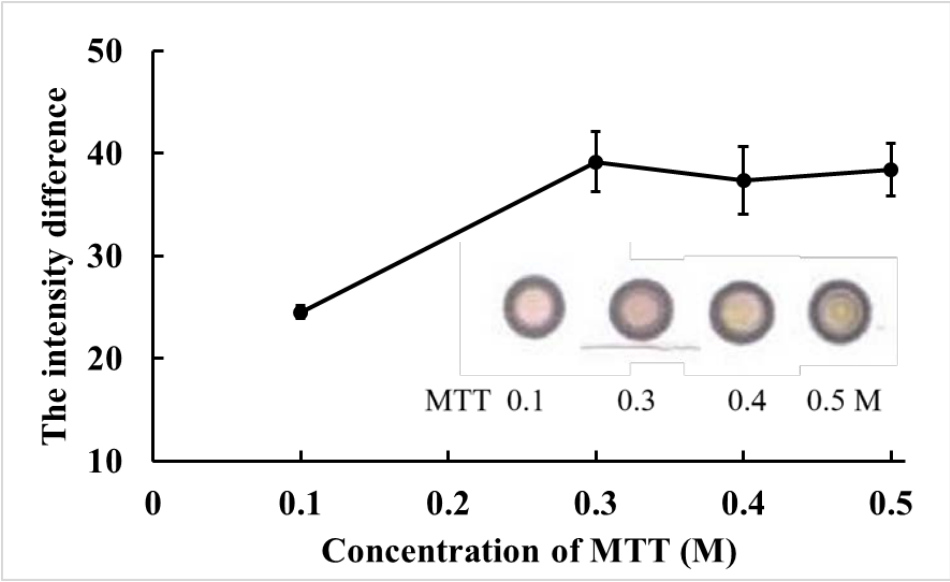

Figure 3A Optimization of MTT concentration at 3 mM PMS, 57 mM NAD+, and 200 μM oxalate. The color intensity was recorded at 30 min analysis time.

NAD+ concentrations were varied from 5 to 57 mM. The results showed that an increase intensity difference was observed as NAD+ concentration was increased. The optimized NAD+ concentration was selected at 40 mM because the intensity difference was not significantly different between 40 and 57 mM as showed in Fig. 4A.

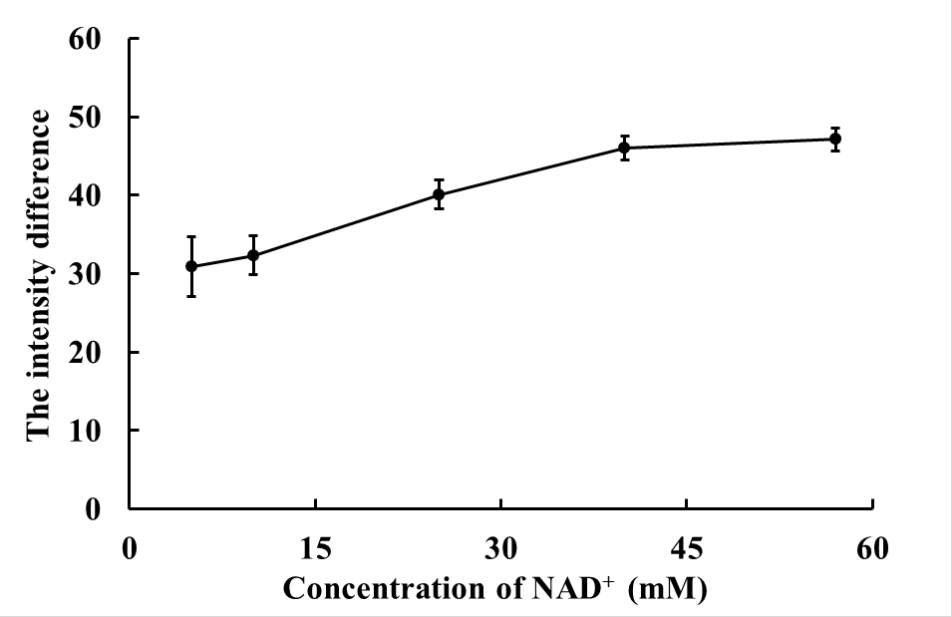

Figure 4A Optimization of NAD+ concentration at 0.3 M MTT, 3 mM PMS, and 200 μM oxalate. The color intensity was recorded at 30 min analysis time.

3.1.2 Effect of analysis time

The chemical and enzyme reaction require time to reach their equilibrium reaction therefore the analysis time after loading sample needs to optimize. Images of the resulting colors were recorded at 5 minutes and then recorded every 15 minutes until it reached 45 minutes of the reaction time. It was observed that the longer reaction time gave the higher intensity difference (Fig. 5A). We selected at 30 min of analysis time to compromise between rapid and sensitive detection of oxalate.

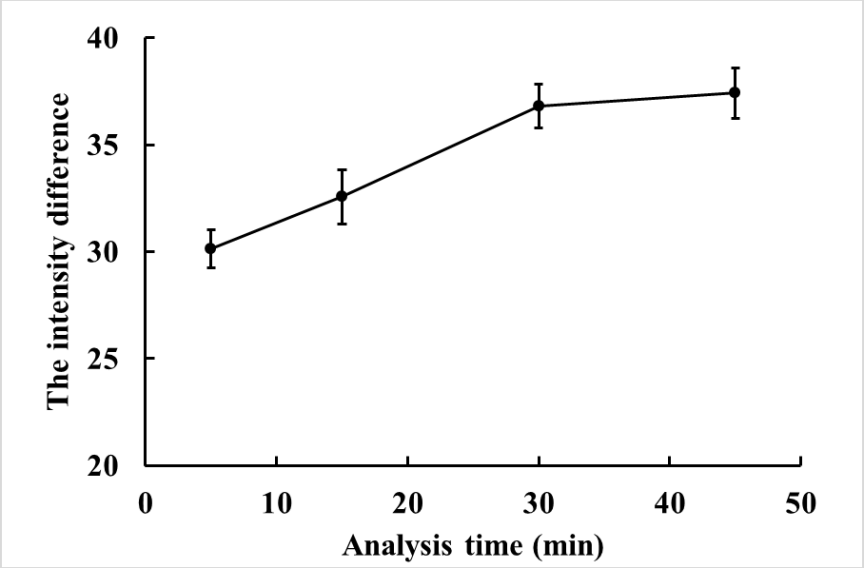

Figure 5A Analysis time study at 0.3 M MTT, 3 mM PMS, 200 μM oxalate, and 57 mM NAD+.

3.2 Analytical Performance

After determining the optimal condition, the linearity between intensity difference and oxalate concentration (0-1000 μmol/L) was demonstrated. The quantitative detection of oxalate was found in the range from 10-1000 μmol/L with linear equation y = 0.0086x + 34.978 and correlation coefficient (R2) = 0.9994 (Fig. 6A). The threshold level of oxalate in human urine 100-300 μmol/L and over 300 μmol/L, respectively for healthy and unhealthy individuals. Our device should therefore be comprehensive for the determination of oxalate in human urine samples. The detection limit was found to be 10 μmol/L by naked eyes. Our linear range and LOD were wider and five times lower than oxalate peroxidase coated on paper-based device (100-2500 μmol/L, LOD = 50 μmol/L). Moreover, our cPAD required lower sample and reagent volume than that report.

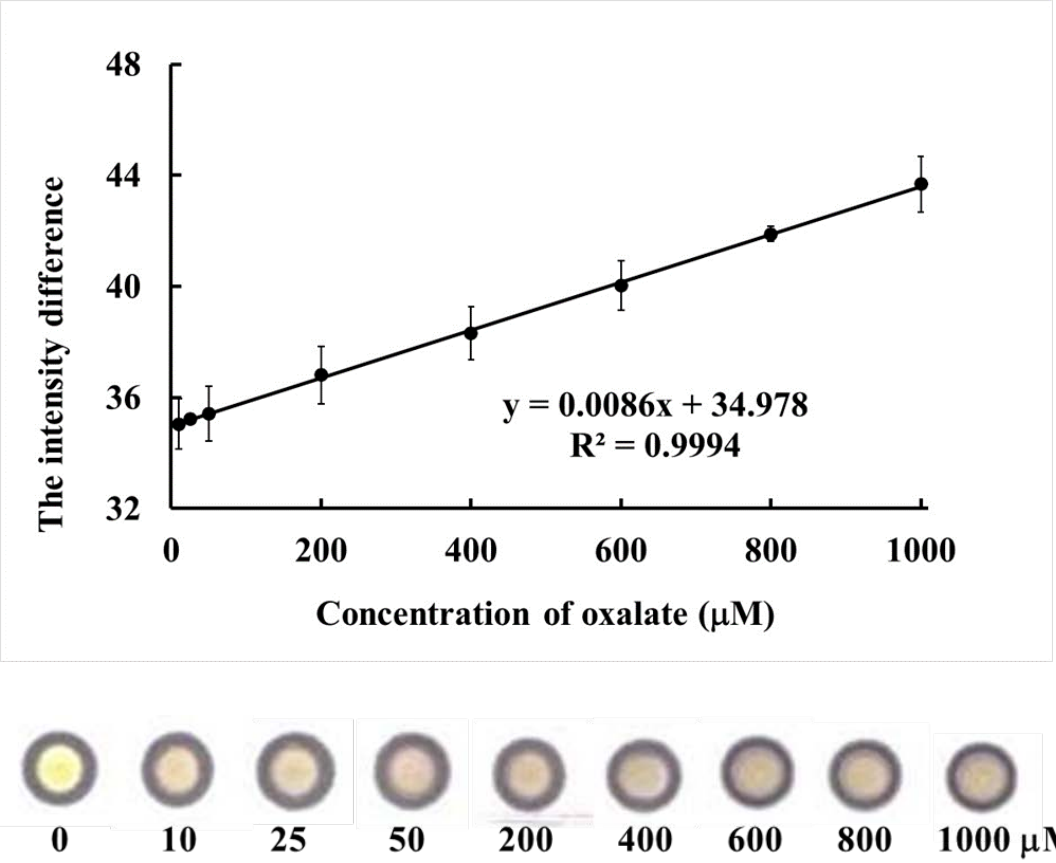

Figure 6A The linearity response under the optimized conditions.

Next, we studied the formate interference due to our assay relating with formate pathway (Fig. 1) and real urine sample containing with formate (0-400 μmol/L for healthy human). Furthermore, formate derived from the metabolism of formaldehyde, several other industrial compounds and some drugs may elevate the urine formate concentration above the normally expected values. The formate concentrations in human urine samples who exposure to chemicals were reported as 100-2000 μmol/L. Hence, the formate concentration in the ranging from 0-2000 μmol/L was also studied to verify in term of formate interference. We found that the intensity difference wasn't significantly different among all formate concentrations (average intensity difference of all formate conc. = 25.249±5.273, n = 12) due to the rapid evaporate of formic acid (Fig. 7A). Although the higher mole of formate was

dropped on cPAD but the enzymatic rate of formate dehydrogenase is slower than the evaporating rate of formic acid. From the equation of linear relationship between oxalate and intensity difference, it obtained the intercept at 34.978 that can subtract average intensity difference of formate at 0-2000 μmol/L. Hence, our cPAD can used for the determination of urinary oxalate without formate interfere under the optimized conditions. The precision expressed as the relative standard deviation (RSD%), obtained from a series of 12 standard samples containing 200 and 400 μmol/L of oxalate, was less than 7%. According to AOAC, Guidelines for Standard Method Performance Requirements, %RSD was limited to be lower than 8%.

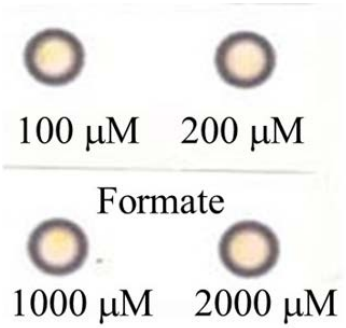

Figure 7A Study of formate interference

Table 1A Determination of urinary oxalate using our cPAD under the optimized conditions.

Artificial urine Sample	**Spiked oxalate (μM)**	**Founded oxalate (μM±SD*), n=3**	**%Recoveries**
S1	200	161±11.1	81
S2	200	165±9.82	83
S3	400	369±8.54	92
S4	400	354±9.70	89

3.3 Applications

In order to evaluate paper-based colorimetric device with real samples, three replicated determinations of oxalate in artificial urine samples spiked with known oxalate standard solution were carried out using the optimized conditions. Artificial urine samples were spiked with known oxalate concentrations at 200 and 400 μmol/L as refer to healthy and unhealthy people, respectively. Recoveries of spiked oxalate in artificial urine samples evaluated by our cPADs were found in the range of 81-92% (table 1A). Our recoveries were lower than 100% in all artificial urine samples because some salts have effect to oxalate decarboxylase activity. However, AOAC limits %recoveries in the ranging 80-110% so our device can be acceptable applied for oxalate determination in artificial urine samples.

PART B: Distance–based Paper Sensor for Determination of Chloride ion Using Silver Nanoparticles

3.1 Principle of Detection

The reaction mechanism for the determination of chloride ions using AgNPs in this work is the redox reaction between H_2O_2 and Ag in the presence of Cl^-. AgNPs without Cl^- could not be oxidized by oxygen (E^o $O2/OH^-$ = +0.40 V) due to the relatively high standard reduction potential of Ag^0 (E^o $Ag+/Ag^0$ = +0.78 V). However, the standard reduction potential of Ag in the presence of Cl^- is decreased (E^o $AgCl/Ag^0$ = +0.22 V) and the standard reduction potential of H_2O_2 is more positive than oxygen (E^o H_2O_2/H_2O = +1.78 V).

The reaction mechanism was tested through the addition of Cl^- in the presence and absence of H_2O_2 using AgNPs-modified paper device. The white color did not appear on the paper device coated by AgNPs with the addition of buffer, Cl^- solution, or H_2O_2 solution. Only the mixture of Cl^- and H_2O_2 gave the white color on paper devices modified AgNPs. These results clearly show the viability of the proposed chemistry for detecting chloride in water.

3.2 Characterization of AgNPs

The change in AgNP size and morphology were first characterized using UV-visible spectroscopy. The maximum absorbance for the AgNPs was found at 403 nm (yellow color solution) as shown in Fig. 1B. The result confirmed the size of the AgNPs (10 nm). In the presence of chloride ions, the absorbance at 403 nm decreased without the appearance of a new peak suggesting etching of the AgNPs with the combination of H_2O_2 and Cl^-.

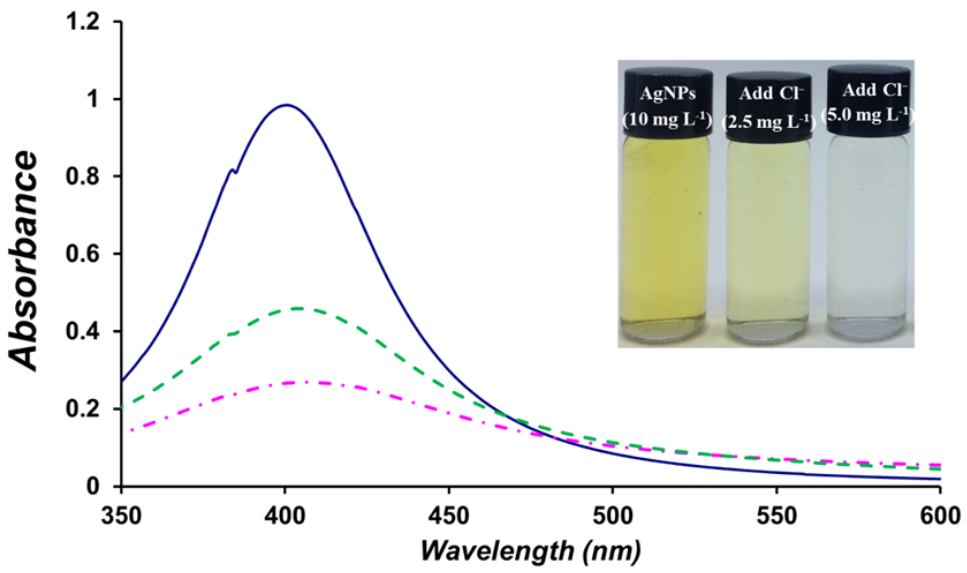

Fig. 1B The UV-visible absorption spectra of the AgNPs. (Insert is photo of the solution AgNPs and a mixture of AgNPs, Cl^- and H_2O_2.)

Next, the morphology AgNPs in presence and absence of the Cl^- and H_2O_2 mixture was confirmed by TEM. TEM images of AgNPs without Cl^- and H_2O_2 showed spherical particles and AgNPs size were found have a 10 nm average diameter (Fig. 2B(a)). TEM images of AgNPs after addition of H_2O_2 and Cl^- showed a change in size to larger sizes (Fig. 2B(b)), similar to those found in solution. Therefore, it was confirmed that AgNPs are etching in the presence of H_2O_2 and Cl^- resulting in the formation of AgCl particles. SEM images of paper before and after adding chloride are shown Figs. 3B(a) and Fig. 3B(b), respectively. The average diameter of AgNPs were higher than AgNPs size before the addition of Cl^-. EDX spectrum demonstrates the elemental composition carbon (C), oxygen (O), silver (Ag), and chloride (Cl) are shown in Fig. 3B(c) and 3B(d). The results confirm the elemental identification of the deposited AgNPs and Cl^- on paper. The AgNPs is oxidized with H_2O_2 and reacts with Cl^- to form the white AgCl precipitate and the precipitate length increased proportionally with the Cl^- concentration.

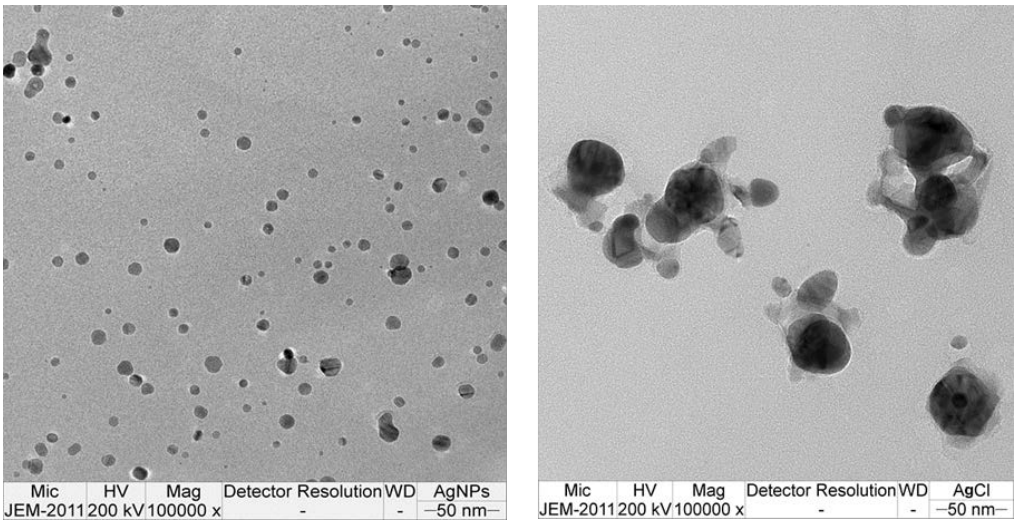

Fig. 2B TEM images of AgNPs (a) without and (b) with Cl^- and H_2O_2. Scale bars are 50 nm.

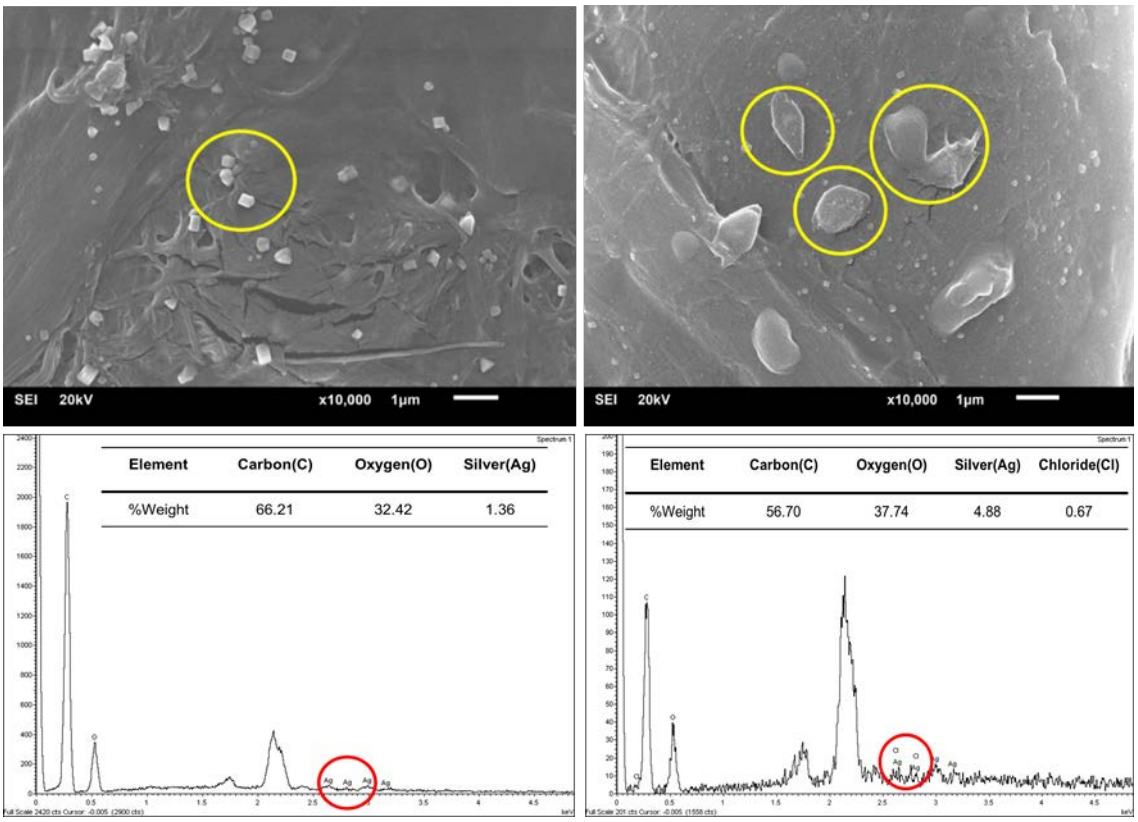

Fig. 3B SEM images of AgNPs on a distance-based paper sensor in the (a) presence and (b) absence of chloride ions. Conformation of elemental silver in a distance-based paper sensor in the (a) presence and (b) absence of chloride ions by EDS spectrum.

3.3 Optimization of the assay conditions

3.3.1 Effect of reaction times

The effect of reaction time was determined by adding the sample to the sample zone and waiting until the reaction was finished. Our assay required at least 25 min because of the time required to flow solution through the channel, and the redox and precipitation reactions to occur. Because of the dramatic change in color, the change can be easily distinguished by naked eye within 30 min. Accordingly, we selected at 30 min as the optimum reaction time.

3.3.2 Effect of pH

In real world sample, pH of samples is variable so the effect of pH on the Cl^- determination was determined using a buffer solution in pH range of 3–10. The study revealed that the pH values did not affect the measurement of Cl^-. This result is not surprising given the stability of AgNPs across a range of pH values.

3.4 Interference studies for the Cl^- detection

In order to determine the selectivity of distance-based devices for detection of chloride, competitive experiments were carried out in the presence of 250 mg L^{-1} Cl^- and interfering ions (F^-, I^-, Br^-, PO_4^{3-}, NO_2^-, NO_3^-, Cr^{3+}, Hg^{2+}, Cd^{2+}, Cu^{2+}, Zn^{2+}, Fe^{3+}, Mn^{2+}, CO_3^{2-} and SO_4^{2-} ions) based on the concentrations commonly found in natural water (1 mg L^{-1} of F^-, I^-, Br^-, Cr^{3+}, Hg^{2+}, Cd^{2+}, Cu^{2+}, Fe^{3+}, and Mn^{2+}, 10 mg L^{-1} of Zn^{2+},

50 mg L^{-1} of PO_4^{3-}, NO_2^- and NO_3^-, and 250 mg L^{-1} of CO_3^{2-} and SO_4^{2-}). The results obtained from the measuring the mixture of Cl^- and the interfering ion were defined as a positive or negative error in the white length that was less than 10% compared to the response of the Cl^- alone (Fig. 4B). However, the concentration of SO_4^{2-} and CO_3^{2-} ions in natural water can be substantially higher than Cl^- depending on the pH, so an additional interference study for these two ions was performed. In this study, a different amount of each interfering ion was added to the 250 mg L^{-1} Cl^- solution. The concentration ratio of Cl^- and the interfering ion was set at 1:1, 1:2, 1:3, 1:4, and 1:5, respectively. At 1:5 ratio of SO_4^{2-} ions did not significantly affect the measurement. However, the 1:3 ratio of CO_3^{2-} did impact the Cl^- measurement, resulting in a higher chloride value. Therefore, carbonate will

interfere when the concentration is >750 mg L^{-1}. Thus, the proposed method provide a high selectivity for chloride detection in natural water.

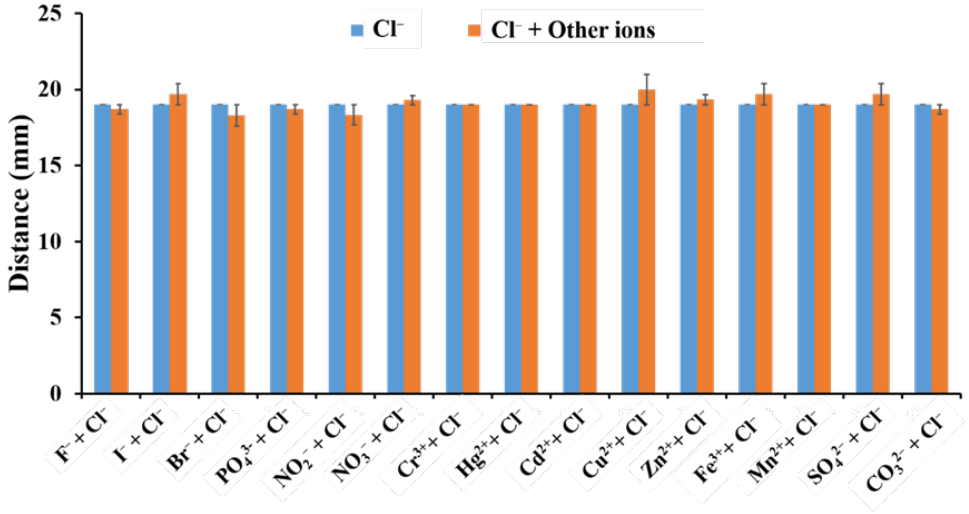

Fig. 4B Responses of AgNPs in the Cl^- and the mixture of Cl^- with other interfering ions. The concentration of Cl^- was 250 mg L^{-1} and mixture other interfering ions based on the concentration available in natural water.

3.5 Analytical performance of the paper-based distance sensor

Using the optimized conditions, a linear calibration curve between distance and Cl^- concentration was obtained in the range of 25 to 1,000 mg L^{-1} (R^2 = 0.9954) as shown in Fig. 5B. The linear range is sufficient for monitoring natural water where the maximum allowable Cl^- level of 250 mg L^{-1} has been established by the World Health Organization (WHO) for drinking and natural waters. Next, the effect of sample/standard solution volume on sensitivity was examined by varying the standard solution volume. We found that the white distance increased when the standard solution volume increased as a result of the increase in moles of Cl^-. It was next found that the limit of detection could be improved by the increasing of standard/sample volume. Hence, the naked-eye detection limit (LOD) of Cl^- in the distance-based device is 0.08 µg and

0.10 µg based on 40 µL and 20 µL of 2 and 5 mg L^{-1} standard solution, respectively. To evaluate the reproducibility of the sensors, the relative standard deviation (% RSD) was

determined using 100, 250 and 500 mg L^{-1} of Cl^{-}. The %RSD of our sensors is 4.51, 3.46 and 2.66, respectively (n =10).

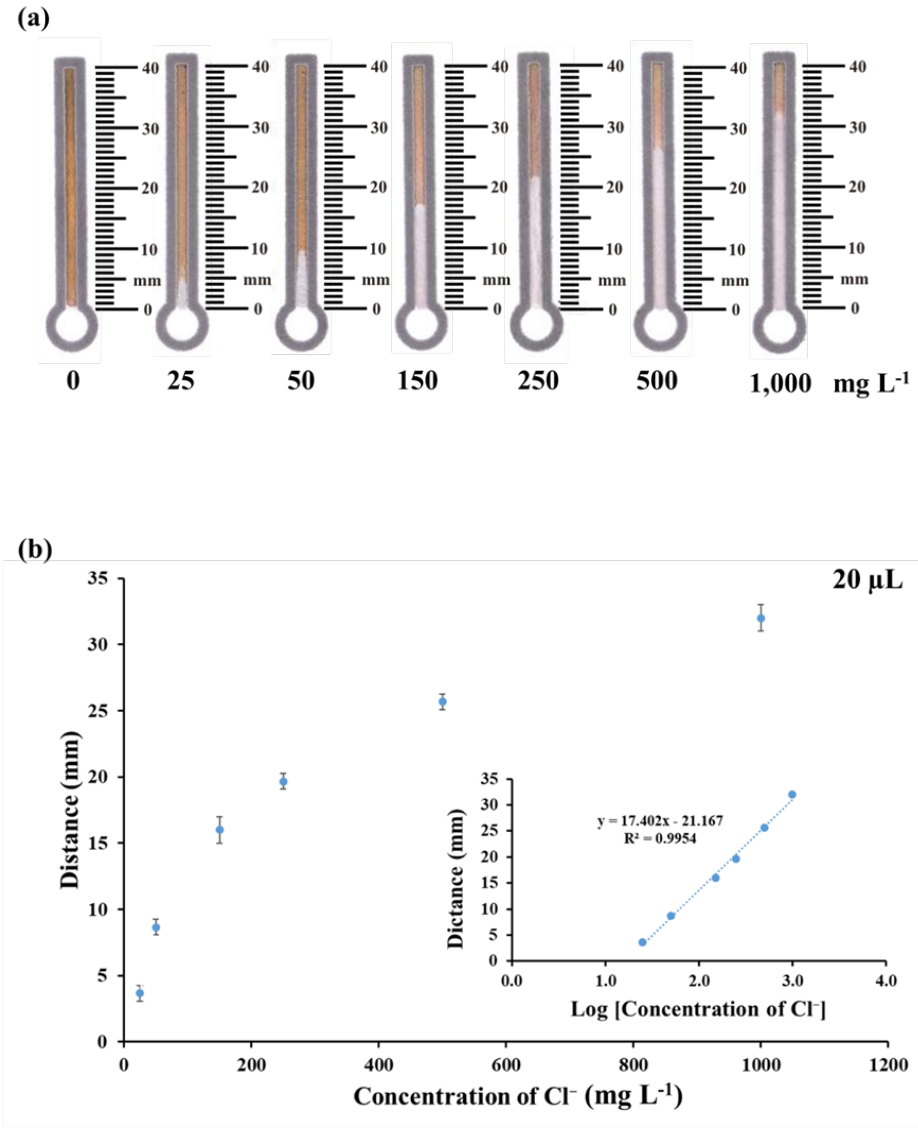

Fig. 5B (a) The distance -based paper sensor device showing the corresponding relationship between increasing color band length and the increasing concentration of the Cl^{-}. (b) The calibration of Cl^{-} concentration between 25 and 1000 mg L^{-1} by using the distance-based devices, n=3.

3.6 Applications for real samples

To validate our assay for the determination of Cl^- in real samples, mineral water from a local supermarket was analyzed for the amount of Cl^- using our assay and a reference standard method (Ion chromatography, IC). The samples were prepared by added with 0.04% (v/v) of H_2O_2 (1:1 v/v of sample: H_2O_2) before addition to the sample zone. The results obtained by the paper-based distance sensor devices were compared by ion chromatography. Chloride in samples 2, 3, and 4 could not be measured using the calibration curve obtained from our standard concentrations (Fig. 5B), but we can increase the mass loading by increasing the volume of the standard/sample to get a lower detection limit. Therefore, we increased the volume of the standard/sample to 40 μL and used the calibration curve between mass of Cl^- and distance for samples 2, 3, and 4. The resulting methods were shown to correspond to the standard method (paired t-test at the 95% confidence level gave t-calculated (0.976) below t-critical at t = 2.776). Consequently, our proposed distance-based device for the determination of chloride ions are acceptable and potentially possible for use with real world samples.

Our device is proposed to be the innovative device for an instrument-free, portable determination of Cl^- by unskilled personnel. To test this proposal, results from standard solution of Cl^- were interpreted by 30 randomly selected chemistry students and out-of-field individuals who were asked to compare results from a commercial chloride test kit (interpret data by the huge of color) and our device (interpret data by the distance of color). Then we compared the percentage of correct answer obtained from 30 untrained individuals. The results indicated that our devices were successfully applied for chloride quantitation by the naked eye of unskilled personnel. Our device had an accuracy of 91-106 %, while the commercial test kit had an accuracy of 40-200 %. The results suggest our approach provides a more accurate result when compared to interpreting data by the huge of color.

Sample		Our method	Standard method
		Found amount (mg L^{-1})	Found amount (mg L^{-1})
Not spiked	Sample 1	94.86 ± 0.00	111.3 ± 0.86
	Sample 2	1.930 ± 0.00*	1.801 ± 0.03
	Sample 3	4.422 ± 0.49*	4.440 ± 0.04
	Sample 4	5.387 ± 0.59*	5.425 ± 0.04
	Sample 5	58.51 ± 4.56	47.56 ± 0.14
100 mg L^{-1} spiked	Sample 1	192.50 ± 15.02	203.13 ± 0.096
	Sample 2	108.28 ± 0.00	98.16 ± 0.067
	Sample 3	108.28 ± 0.00	100.99 ± 0.32
	Sample 4	103.59 ± 7.74	102.31 ± 0.043
	Sample 5	154.40 ± 11.52	142.62 ± 0.27
200 mg L^{-1} spiked	Sample 1	286.31 ± 22.33	288.64 ± 0.22
	Sample 2	201.17 ± 15.02	191.88 ± 0.27
	Sample 3	192.50 ± 15.01	203.06 ± 0.12
	Sample 4	201.17 ± 15.01	198.08 ± 0.43
	Sample 5	250.82 ± 19.56	231.16 ± 0.59

CHAPTER IV

CONCLUSIONS AND FUTURE PERSPECTIVE

In part A, we have developed paper-based colorimetric device, which is easy to use for the determination of urinary oxalate with highly sensitivity (LOD = 10 μM), acceptable repeatability (< 7% RSD) and rapidity (analysis time = 30 min.). Moreover, the analysis was inexpensive and did not require complexed equipment or extensive training of users. Our cPAD has been successfully applied to the determination of levels of oxalate in artificial urine samples (81-92 %recoveries). Our device therefore suggested a path for the development of a portable diagnostic assay that may be useful in remote setting, and important for monitoring the point-of-care health diagnosis of kidney stone disease.

In summary of part B, the distance-based device was successfully developed for the inexpensive, easy-to-use, instrument-free, portable determination of Cl^- using AgNPs by unskilled personnel. This analysis is based on the oxidative etching of the silver nanoparticles (AgNPs) in the presence of H_2O_2 and Cl^- to form AgCl, forming a white color band whose length is proportional to the quantity of Cl^-. Because of the strong change in color, the result can be easily observed by naked eye. Our proposed device can give sub microgram (0.08 μg) detection limits (LOD) depending on the volume of sample solution. Furthermore, no significant differences for the amount of Cl^- in real samples between using our devices and the traditional method were observed. Our device could be applied to low-level detection of Cl^- in real samples by unskilled personnel and with no instrumentation.

ภาคผนวก

Output ที่ได้จากโครงการคือ International Journal Publication จำนวน 2 ฉบับ ตามภาคผนวกแนบนี้

Analyst

PAPER

View Article Online
View Journal | View Issue

Cite this: *Analyst*, 2018, **143**, 3867

A distance-based paper sensor for the determination of chloride ions using silver nanoparticles†

Kamonchanok Phoonsawat,[a] Nalin Ratnarathorn,[a] Charles S. Henry [b] and Wijitar Dungchai *[a]

We report for the first time the development of a distance-based paper sensor for a simple, inexpensive, instrument-free, and portable determination of chloride ions. Our analysis reaction is based on the oxidative etching of silver nanoparticles (AgNPs) to form AgCl in the presence of Cl^- and H_2O_2. H_2O_2 reacts with AgNPs in the channel of the paper device and Cl^- in the sample forming a white precipitate (AgCl) where the white color band length is proportional to the Cl^- concentration. Quantification of Cl^- is achieved by measuring the length of the white color band using a ruler printed on the side of the channel. Under optimal conditions, the distance-based paper sensor was characterized by a working range of 25–1000 mg L^{-1} (R^2 = 0.9954) and the naked eye detection limit (LOD) was 2 mg L^{-1} (0.08 μg). Our sensor was found to be reproducible with a relative standard deviation of less than 4.51% (n = 10). The levels of Cl^- in real water samples measured using our proposed device were within the error of the values measured using traditional tests but without the need for any external instrumentation. Therefore, our proposed method presents acceptable accuracy, precision, and high selectivity for point of need monitoring of Cl^- in real water samples.

Received 11th April 2018,
Accepted 27th June 2018

DOI: 10.1039/c8an00670a

rsc.li/analyst

1. Introduction

Chloride is an anion commonly found in water. In general, chloride combines with calcium, magnesium, or sodium to form various salts. Chloride gives water a salty taste at high concentrations. Taste thresholds for chloride depend on the associated cation and are in the range of 200–300 mg L^{-1} for sodium, potassium and calcium chloride.[1] Chloride at high concentrations may also affect agricultural crops because salinity can cause dehydration and cause plant death.[2] Moreover, high levels of sodium chloride increase the potential for corrosive water damage to plumbing fixtures causing toxic metals to be released into water.[3] The maximum allowable Cl^- level of 250 mg L^{-1} has been established by the World Health Organization (WHO) for drinking water and natural water. Therefore, the amount of chloride in water needs to be monitored regularly. Several methods exist for Cl^- determination, including titration,[4] photometry,[5] electrochemistry,[6–9] spectrophotometry[10–12] and ion chromatography.[13–15] Although they provide high precision and accuracy, they also require relatively expensive instrumentation and the transmission of data from on-site to experts. Hence, our aim is to develop a low-cost, simple, and portable device for measuring chloride levels by unskilled personnel, which can be used at the point-of-need.

Microfluidic paper-based analytical devices (μPADs) have gained much attention for point-of-need monitoring due to their simplicity, low sample and reagent consumption, low cost, and portability. μPADs have been developed for medical diagnostics,[16–20] food contamination,[21–23] and environmental monitoring.[24–26] The most common detection pattern used in μPADs is colorimetry which distinguishes the changes in color hue and/or intensity to quantify the analytes. Although the colorimetric method is popular, it has some limitations including different visual perception of color from one person to another and lighting effects on color readings.[27,28] In addition, precise and accurate quantification requires the use of peripheral technologies such as digital scanners, cameras or other optical sensors/electrochemical sensors. Thus, some researchers have developed distance-based detection on μPADs which quantify analytes based on the color length without the need for any

[a]*Organic Synthesis, Electrochemistry & Natural Product Research Unit, Department of Chemistry, Faculty of Science, King Mongkut's University of Technology Thonburi, Prachautid Road, Thungkru, Bangkok, 10140, Thailand.*
E-mail: wijitar.dun@kmutt.ac.th; Fax: +66-02-470-8840; Tel: +66-02-470-9553
[b]*Departments of Chemistry and Chemical & Biological Engineering and School of Biomedical Engineering, Colorado State University, Fort Collins, CO 80523, USA*
†Electronic supplementary information (ESI) available. See DOI: 10.1039/c8an00670a

external instrumentation.[29–34] Distance-based devices generally consist of an inlet for adding samples and a flow channel containing a specific colorimetric reagent for the substance of interest. When a sample or standard solution is added to the inlet, it reacts with the indicator on the device until all of the analyte is consumed. The result is a colored band whose length is proportional to the amount of analyte available in the sample. Measuring the color length gives less error than measuring the color intensity by means of computer software. The distance-based device has been applied in several varieties of clinical and environmental studies such as the determination of glucose, nickel, and glutathione,[29] the study of aerosol oxidative activity,[30] the lactoferrin detection in human tear samples,[31] multiplexed analysis of all three metals (Ni, Cu, and Fe),[32] and the detection of Cu^{2+}.[34]

Recently, metallic nanoparticles including gold nanoparticles (AuNPs) and silver nanoparticles (AgNPs) have been used as colorimetric agents for μPADs.[35–39] However, the synthesis of AuNPs requires expensive chemicals so the AgNPs are more popular than AuNPs when cost is a significant consideration. Compared to AuNPs, AgNPs display stronger surface plasmon absorption (SPR) resonance with an ultrahigh extinction coefficient, which in principle promises a wider range of potential applications. AgNPs react strongly with inorganic ligands such as sulfide and chloride once the silver is oxidized. Chloride (Cl^-) is a ubiquitous ligand with a strong affinity for oxidized silver. In 2018, the determination of chloride by silver nanoprisms using a paper-based colorimetric sensor has been reported.[40]

In this work, we report a non-instrumented chloride analysis using distance-based detection on μPADs. The designed device resembles a thermometer and creates a flow channel using a wax barrier. Silver nanoparticles (AgNPs) are deposited along the flow channel and dried at room temperature. When Cl^- is added to the device, it flows through the channel and reacts with the AgNPs. A visible color change of AgNPs from dark-yellow to white as a result of AgCl precipitation was observed with the naked eye, with the length of the white color band being proportional to the quantity of Cl^-. Quantitative analysis can be achieved by measuring the distance of the colored zone using a ruler printed on the side of the channel. Our proposed device provides low cost, easy-to-use, and portable determination of chloride by unskilled personnel. Moreover, it can be applied to the detection of chloride ions in real samples, providing satisfactory precision and accuracy when compared to traditional chloride assays.

2. Experimental

2.1 Chemicals and materials

Silver nanoparticles (1000 mg L^{-1}) with a diameter of 10 nm were obtained from the Sensor Research Unit at the Department of Chemistry, Chulalongkorn University, Thailand. Standard solutions of cations (Cr^{3+}, Mn^{2+}, Cd^{2+}, Cu^{2+}, Zn^{2+} and Fe^{3+} in 2% HNO_3 and Hg^{2+} in 12% HNO_3) were purchased from Sigma-Aldrich (AA grade). Standard anions (NaCl, $NaHCO_3$, $NaNO_3$, $NaNO_2$, NaF, KI, KBr, NaH_2PO_4 and $MgSO_4$) were purchased from Merck, Germany. All chemicals used in the experiment were analytical reagents (AR grade) and solutions were prepared using highly pure water from Milli-Q ($R \geq 18$ MΩ cm). Whatman No.1 filter paper was bought from Cole-Parmer (Vernon Hills, IL).

2.2. Instrumentation

UV–visible absorption spectra were recorded with a UV-visible spectrometer (Lambda 35, Perkin15 Elmer Instruments, USA) using quartz cuvettes (1.0 cm path length) for characterizing silver nanoparticles (AgNPs). The shapes and particle sizes were determined using a transmission electron microscope (TEM, JEOL, JEM-2010) and a scanning electron microscope (SEM, JEOL, JSM-6610 LV).

2.3. Preparation of the silver nanoparticles

A silver nanoparticle (AgNP) solution was prepared according to the previously reported method.[41] Briefly, a solution of silver nitrate ($AgNO_3$) and a reducing agent was prepared by dissolving them in starch solution. After this, the $AgNO_3$ solution was added to the reducing agent solution at a flow rate of 2 mL s^{-1} under vigorous stirring at room temperature. The colorless solution became dark yellow, indicating the formation of small silver nanoparticles. After stirring for 30 min, the synthesized AgNPs were boiled for 2 h and cooled down to room temperature for 12 h. The shape and particle size distributions of AgNPs were confirmed by UV–visible spectroscopy, scanning electron microscopy (SEM) and transmission electron microscopy (TEM). The absorbance spectra were recorded using a UV-visible spectrophotometer in the wavelength range of 350–600 nm.

2.4 Device fabrication and operation

The operational concept for distance-based detection is shown in Fig. 1. Briefly, the pattern of the device was designed in the shape of a thermometer using CorelDraw and consisted of a sample inlet (diameter 7 mm) and a straight channel for the detection zone with a width of 3.5 mm and a channel length of 40 mm. The designed width of the hydrophobic wax was 3 pt. The design was printed on Whatman No.1 filter paper using a wax printer (Xerox ColorQube 8870, Japan). After printing, the device was placed in an oven for 2 min at 150 °C and then cooled to room temperature. The back side of the device was sealed with tape to prevent solution leakage through the device. The AgNPs were spotted onto the detection channel using a pipette and allowed to dry. After this, 20 μL of standard or sample solution mixed with H_2O_2 was added to the sample zone, where it was carried by capillary action along the flow channel and reacted with AgNPs along the detection channel (25 ± 3 °C).

2.5 Optimization of distance-based devices

To optimize the distance-based devices, the effect of reaction times and pH (pH range 3 to 10) was evaluated. For this study, 250 mg L^{-1} of Cl^- was used to obtain optimal conditions for Cl^- detection because the maximum allowable Cl^- level established by the World Health Organization (WHO) for drinking water and

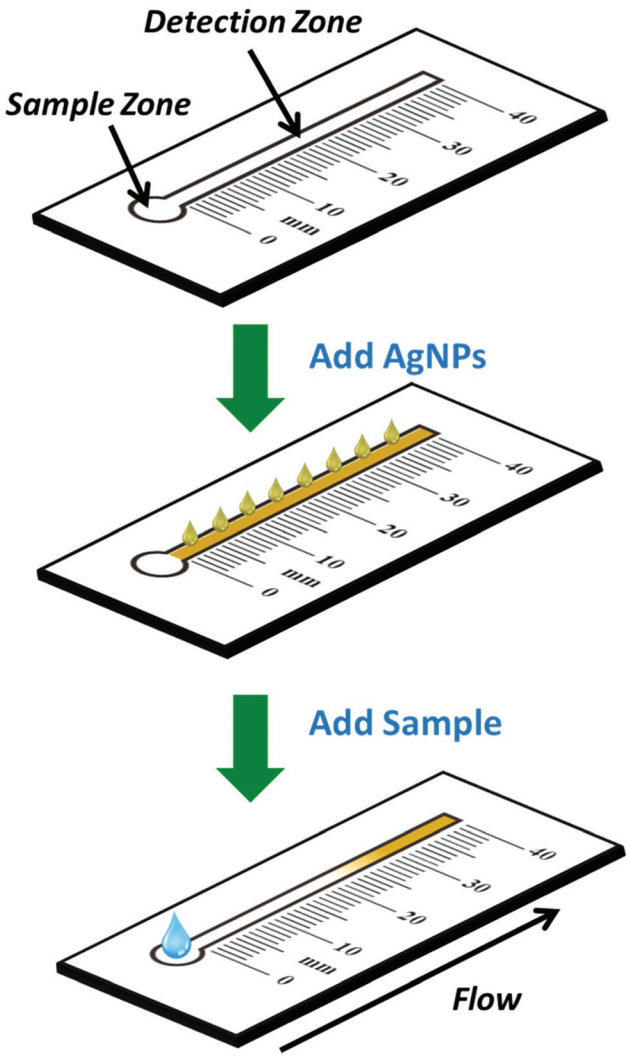

Fig. 1 Schematic design of the distance-based paper sensor designs and general analytical methods.

natural water is 250 mg L^{-1}. The optimum ratios of chloride and hydrogen peroxide (Cl^- : H_2O_2) were studied by using the ratio of 250 mg L^{-1} Cl^- and 0.04% (v/v) H_2O_2 at 1 : 1, 2 : 1 and 3 : 1 by v/v.

2.6 Applications for real samples

The mineral water samples were purchased from a local supermarket. One part was analyzed by ion chromatography (Dionex Integrion HPIC, Thermo-Fisher Scientific Inc., USA). For the second part, water samples were immediately mixed with 0.04% (v/v) of H_2O_2 (ratio 1 : 1 v/v) prior to analysis with our device.

3. Results and discussion

3.1 Principle of detection

The reaction mechanism for the determination of chloride ions using AgNPs in this work is the redox reaction between H_2O_2 and Ag in the presence of Cl^-. AgNPs without Cl^- could not be oxidized by oxygen (E° O_2/OH^- = +0.40 V) due to the relatively high standard reduction potential of Ag^0 (E° Ag^+/Ag^0 = +0.78 V). However, the standard reduction potential of Ag in the presence of Cl^- is decreased (E° $AgCl/Ag^0$ = +0.22 V) and the standard reduction potential of H_2O_2 is more positive than that of oxygen (E° H_2O_2/H_2O = +1.78 V) as shown in reaction 1.

Reaction 1.

$$AgCl_{(s)} + e^- \rightleftharpoons Ag^0 + Cl^- \quad E^\circ = +0.22\ V$$

$$H_2O_2 + 2H^+ + 2e^- \rightarrow 2H_2O \quad E^\circ = +1.78\ V$$

$$H_2O_2 + 2Ag^0 + 2Cl^- + 2H^+ \rightleftharpoons 2AgCl_{(s)} + 2H_2O$$

The reaction mechanism was tested through the addition of Cl^- in the presence and absence of H_2O_2 using a AgNP-modified paper device. The white color band did not appear on the paper device coated with AgNPs with the addition of buffer (Fig. S1(a)†), Cl^- solution (Fig. S1(b)†), or H_2O_2 solution (Fig. S1(c)†). Only the mixture of Cl^- and H_2O_2 gave the white color band on the paper device modified with AgNPs (Fig. S1(d)†) based on the redox reaction given in reaction (1). These results clearly show the viability of the proposed chemistry for detecting chloride in water.

3.2 Characterization of AgNPs

The change in AgNP size and morphology was first characterized using UV-visible spectroscopy. The maximum absorbance for the AgNPs was found at 403 nm (yellow color solution) as shown in Fig. 2. The result confirmed the size of the AgNPs (10 nm). In the presence of chloride ions, the absorbance at 403 nm decreased without the appearance of a new peak suggesting etching of the AgNPs with the combination of H_2O_2 and Cl^-.

Next, the morphology of AgNPs in the presence and absence of the Cl^- and H_2O_2 mixture was confirmed by TEM.

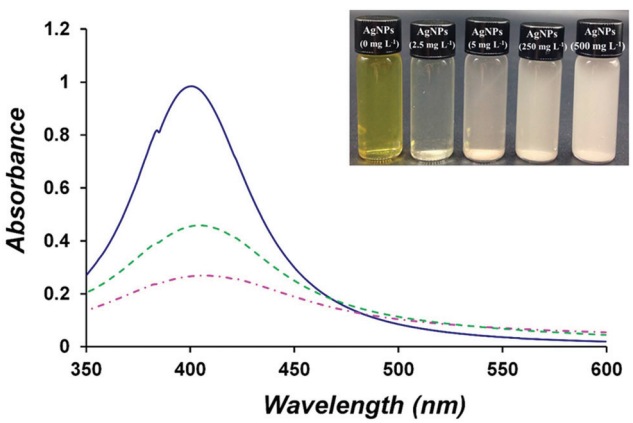

Fig. 2 The UV-visible absorption spectra of the AgNPs. Solid line, dashed line and dotted line represent AgNPs, AgNPs mixed with H_2O_2 and Cl^- at 2.5 and 5 mg L^{-1}, respectively. (Insert is the photograph of the AgNP solution and a mixture of AgNPs, H_2O_2 and Cl^- at 0, 2.5, 5, 250, and 500 mg L^{-1}.)

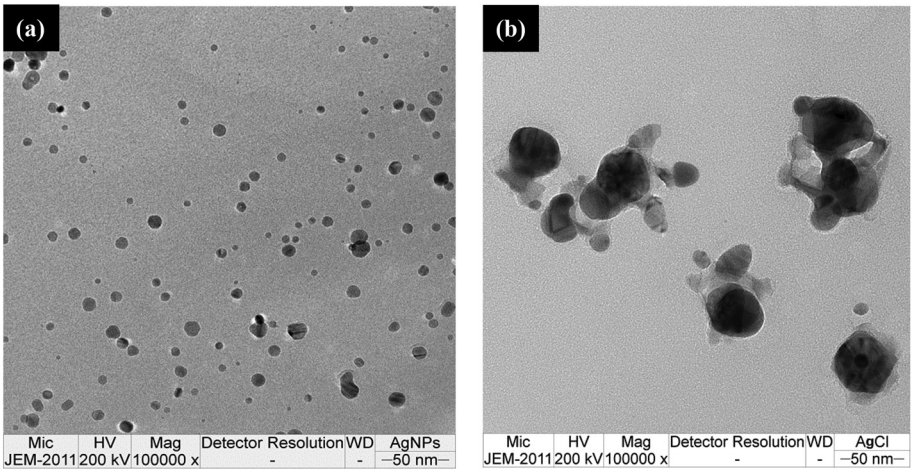

Fig. 3 TEM images of AgNPs (a) without and (b) with Cl^- and H_2O_2. Scale bars are 50 nm.

The TEM images of AgNPs without Cl^- and H_2O_2 showed spherical particles and AgNPs were found to have an average diameter of 10 nm (Fig. 3a). The TEM images of AgNPs after the addition of H_2O_2 and Cl^- showed an increase in size (Fig. 3b), similar to those found in solution (Fig. 2 insert). Therefore, it was confirmed that AgNPs are being etched in the presence of H_2O_2 and Cl^- resulting in the formation of AgCl particles. The SEM images of the paper before and after adding chloride are shown in Fig. 4a and b, respectively. The average diameter of AgNPs was higher than that of AgNPs before the addition of Cl^-. The EDX spectrum demonstrates the elemental composition of carbon (C), oxygen (O), silver (Ag), and chloride (Cl) as shown in Fig. 4c and d. The results confirm the elemental identification of the deposited AgNPs and Cl^- on the paper. The AgNPs are oxidized with H_2O_2 and react with Cl^- to form the white AgCl precipitate and the precipitate length increased proportionally with the Cl^- concentration.

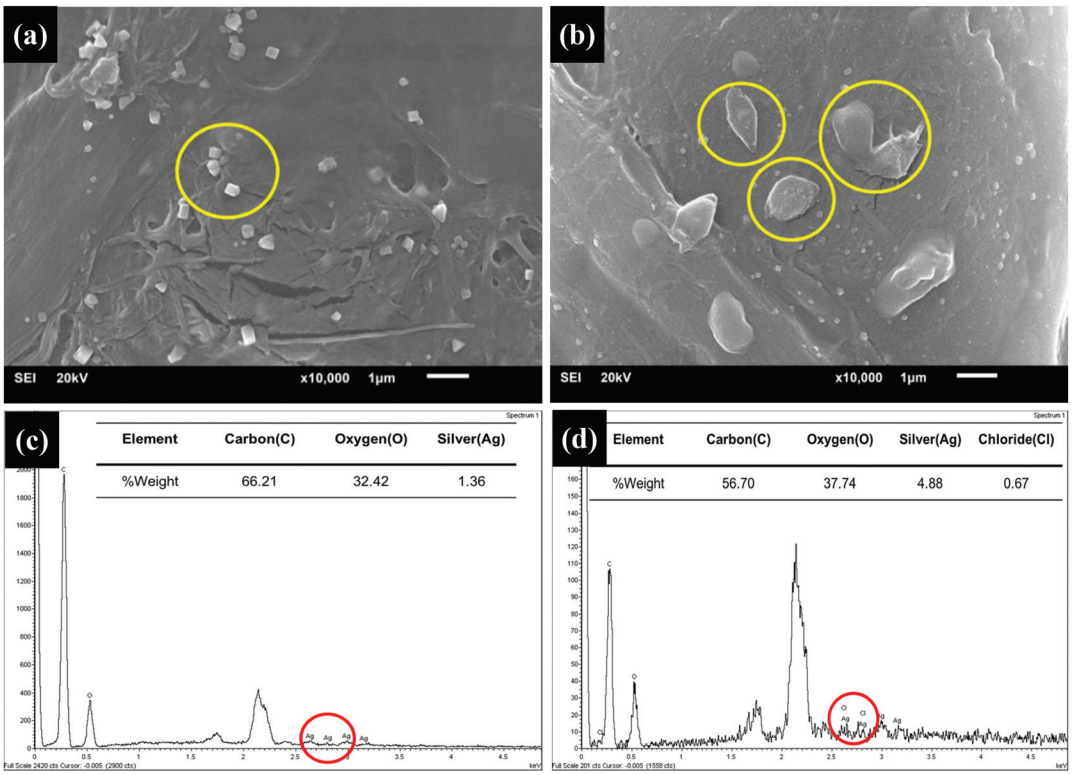

Fig. 4 SEM images of AgNPs on a distance-based paper sensor in the (a) absence and (b) presence of chloride ions. Conformation of elemental silver in a distance-based paper sensor in the (c) absence and (d) presence of chloride ions by EDS spectrum.

3.3 Optimization of the assay conditions

3.3.1 Effect of reaction times. The effect of reaction times was determined by adding the sample to the sample zone and waiting until the reaction was complete. Our assay required at least 25 min because a long time is required for the solution to flow through the channel, enabling the redox and precipitation reactions to occur. Because of the dramatic change in color, the change can be easily distinguished with the naked eye within 30 min (data not shown). Accordingly, we selected 30 min as the optimum reaction time.

3.3.2 Effect of pH. In real world samples, the pH of samples is variable so the effect of pH on Cl^- determination was determined using a buffer solution in the pH range of 3–10. The study revealed that the pH values did not affect the measurement of Cl^- (Fig. S2†). This result is not surprising given the stability of AgNPs across a range of pH values.

3.4 Interference studies for Cl^- detection

In order to determine the selectivity of the distance-based device for the detection of chloride, competitive experiments were carried out in the presence of 250 mg L^{-1} Cl^- and interfering ions (F^-, I^-, Br^-, PO_4^{3-}, NO_2^-, NO_3^-, Cr^{3+}, Hg^{2+}, Cd^{2+}, Cu^{2+}, Zn^{2+}, Fe^{3+}, Mn^{2+}, CO_3^{2-} and SO_4^{2-} ions) based on the concentrations commonly found in natural water (1 mg L^{-1} of F^-, I^-, Br^-, Cr^{3+}, Hg^{2+}, Cd^{2+}, Cu^{2+}, Fe^{3+}, and Mn^{2+}, 10 mg L^{-1} of Zn^{2+}, 50 mg L^{-1} of PO_4^{3-}, NO_2^- and NO_3^-, and 250 mg L^{-1} of CO_3^{2-} and SO_4^{2-}). The results obtained from measuring the mixture of Cl^- and the interfering ions were defined as a positive or negative error in the white color band length which was less than 10% compared to the response of Cl^- alone (Fig. 5). However, the concentration of SO_4^{2-} and CO_3^{2-} ions in natural water can be substantially higher than Cl^- depending on the pH, so an additional interference study for these two ions was performed. In this study, a different amount of each interfering ion was added to the 250 mg L^{-1} Cl^- solution. The concentration ratios of Cl^- and the interfering ions were set at 1 : 1, 1 : 2, 1 : 3, 1 : 4, and 1 : 5. The effect of the interference ratio is shown in Table 1, the 1 : 5 ratio of SO_4^{2-} ions did not significantly affect the measurement. However, the 1 : 3 ratio of CO_3^{2-} did impact the Cl^- measurement, resulting in a higher chloride value. Therefore, carbonate will interfere when the concentration is ≥750 mg L^{-1}. Thus, the proposed method provides a high selectivity for chloride detection in natural water.

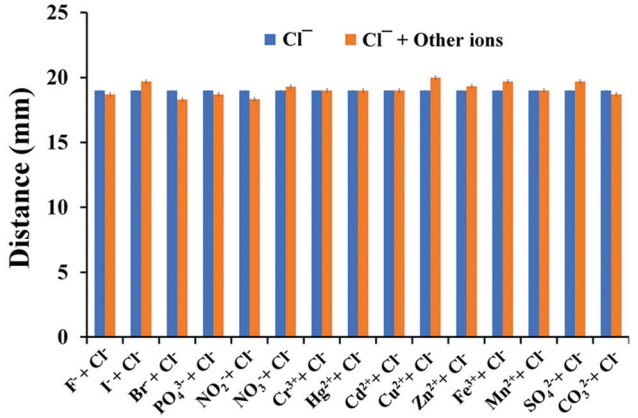

Fig. 5 Responses of AgNPs in Cl^- and the mixture of Cl^- with other interfering ions. The concentration of Cl^- was 250 mg L^{-1} and that of the mixture with other interfering ions is based on the concentration available in natural water.

Table 1 The actual *vs.* measured concentration of Cl^- in varying ratios with other interfering ions

Cl^- : other ions	Ratio	Actual (mg L^{-1})	Measured (mg L^{-1}) $n = 3$	Recovery (%)
Cl^- : SO_4^{2-}	1 : 1	250	233.4 ± 30.8	93
	1 : 2	250	266.5 ± 35.2	106
	1 : 3	250	243.0 ± 19.0	97
	1 : 4	250	254.0 ± 19.0	102
	1 : 5	250	233.4 ± 30.8	93
Cl^- : CO_3^{2-}	1 : 1	250	222.5 ± 16.6	89
	1 : 2	250	225.0 ± 43.8	90
	1 : 3	250	396.3 ± 52.3	158
	1 : 4	250	377.7 ± 28.2	151
	1 : 5	250	471.0 ± 36.7	188

3.5 Analytical performance of the paper-based distance sensor

Using the optimized conditions, a linear calibration curve between the distance and Cl^- concentration was obtained in the range of 25 to 1000 mg L^{-1} (R^2 = 0.9954) as shown in Fig. 6. The linear range is sufficient for monitoring natural water where the maximum allowable Cl^- level of 250 mg L^{-1} has been established by the World Health Organization (WHO) for drinking and natural waters. Next, it was found that the limit of detection could be improved by increasing the standard/sample volume. Hence, the naked-eye detection limit (LOD) values of Cl^- in the distance-based device are 0.08 μg and 0.10 μg based on 40 μL and 20 μL of 2 and 5 mg L^{-1} standard solution, respectively (Fig. S3(a and b)†). To evaluate the reproducibility of the sensor, the relative standard deviation (% RSD) was determined using 100, 250 and 500 mg L^{-1} of Cl^-. The %RSD of our sensor is 4.51, 3.46 and 2.66, respectively (n = 10). Moreover, our system still works in the case of adding a non well-defined volume (*e.g.* a few drops) of a H_2O_2 solution, which would eliminate the need for volumetric steps and simplify the procedure (Fig. S4†).

3.6 Applications for real samples

To validate our assay for the determination of Cl^- in real samples, mineral water from a local supermarket was analyzed for determining the amount of Cl^- using our assay and a reference standard method (ion chromatography, IC).[14] The samples were prepared by adding 0.04% (v/v) of H_2O_2 (1 : 1 v/v of sample:H_2O_2) before addition to the sample zone. The results obtained by the paper-based distance sensor device were compared with those obtained by ion chromatography as presented in Table 2. Chloride in samples 2, 3, and 4 could not be measured using the calibration curve obtained from our standard concentrations (Fig. 6), but we can increase the

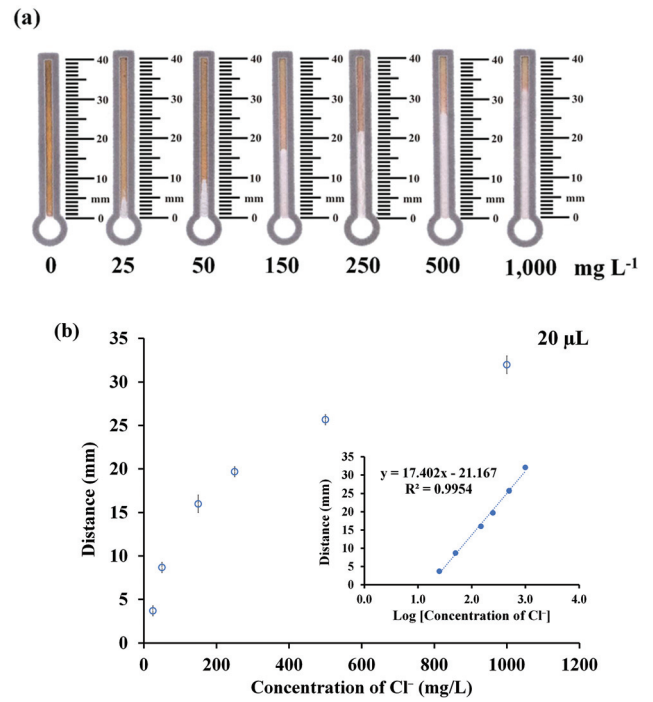

Fig. 6 (a) The distance-based paper sensor showing the corresponding relationship between the increasing color band length and the increasing concentration of Cl^-. (b) The calibration of Cl^- concentration between 25 and 1000 mg L^{-1} using the distance-based paper sensor, n = 3.

Table 2 Determination of Cl^- in real samples by the proposed method compared with the standard method (IC)

Sample		Our method Found amount (mg L^{-1})	Standard method Found amount (mg L^{-1})
Not spiked	Sample 1	94.86 ± 0.00	111.3 ± 0.9
	Sample 2	1.930 ± 0.00[a]	1.801 ± 0.03
	Sample 3	4.422 ± 0.49[a]	4.440 ± 0.04
	Sample 4	5.387 ± 0.59[a]	5.425 ± 0.04
	Sample 5	58.51 ± 4.56	47.56 ± 0.14
100 mg L^{-1} spiked	Sample 1	192.5 ± 15.0	203.1 ± 0.1
	Sample 2	108.3 ± 0.0	98.16 ± 0.07
	Sample 3	108.3 ± 0.0	101.0 ± 0.3
	Sample 4	103.6 ± 7.7	102.3 ± 0.0
	Sample 5	154.4 ± 11.5	142.6 ± 0.3
200 mg L^{-1} spiked	Sample 1	286.3 ± 22.3	288.6 ± 0.2
	Sample 2	201.2 ± 15.0	191.9 ± 0.3
	Sample 3	192.5 ± 15.0	203.1 ± 0.1
	Sample 4	201.2 ± 15.0	198.1 ± 0.4
	Sample 5	250.8 ± 19.6	231.1 ± 0.6

[a] Calibration curve at 40 µL (Fig. S3(a)).

mass loading by increasing the volume of the standard/sample to obtain a lower detection limit. Therefore, we increased the volume of the standard/sample to 40 µL and used the calibration curve between the mass of Cl^- and distance (Fig. S3(a)†) for samples 2, 3, and 4. The resulting methods were shown to correspond to the standard method (paired t-test at the 95% confidence level gave $t_{calculated}$ (0.976) below $t_{critical}$ at t = 2.776). Consequently, our proposed distance-based device for the determination of chloride ions is acceptable and potentially possible for use with real world samples.

Our device is proposed to be an innovative device for an instrument-free and portable determination of Cl^- by unskilled personnel. To test this proposal, 30 randomly selected chemistry students and out-of-field individuals performed the entire assay and interpreted the results from the standard solution of Cl^- by comparing the results obtained using a commercial chloride test kit (data were interpreted based on the hue of color) with those obtained using our device (data were interpreted based on the distance of color). Then we compared the percentage of correct answers obtained from 30 untrained individuals (Table S1†). The results indicated that our device was successfully applied for chloride quantitation with the naked eye of unskilled personnel. Our device had an accuracy of 91–106%, while the commercial test kit had an accuracy of 40–200%. The results suggest that our approach provides a more accurate result compared to the interpretation of data based on the hue of color.

4. Conclusions

In summary, the distance-based paper sensor was successfully developed for the inexpensive, easy-to-use, instrument-free, and portable determination of Cl^- using AgNPs by unskilled personnel. This analysis is based on the oxidative etching of the silver nanoparticles (AgNPs) in the presence of H_2O_2 and Cl^- to form AgCl, forming a white color band whose length is proportional to the quantity of Cl^-. Because of the strong change in color, the result can be easily observed with the naked eye. Our proposed device can give sub microgram (0.08 µg or 2 mg L^{-1}) detection limits (LODs) depending on the volume of sample solution. Furthermore, no significant differences for the amount of Cl^- in real samples between using our device and the traditional method were observed. Our device could be applied to the low-level detection of Cl^- in real samples by unskilled personnel and with no instrumentation.

Conflicts of interest

There are no conflicts to declare.

Acknowledgements

Wijitar Dungchai gratefully acknowledges the financial support from the Thailand Research Fund through MRG6080171, the Innovation and Partnerships Office, and the King Mongkut's University of Technology Thonburi.

References

1 W. H. Organization, *Guidelines for Drinking-water Quality*, World Health Organization, 4th edn, 2011.

2 A. Sheldon, N. W. Menzies, H. B. So and R. Dalal, presented in part at the Australian New Zealand Soils Conference, University of Sydney, Australia, 5–9 December 2004, 2004.
3 N. H. D. o. E. Services, *Environmental Fact Sheet*, Departament of Environmental Services, 2010, pp. 3–5.
4 F. E. CLARKE, *Anal. Chem.*, 1950, **22**(4), 553–555.
5 D. M. Zall, D. Fisher and M. Q. Garner, *Anal. Chem.*, 1956, **28**(11), 1665–1668.
6 S. Dong and G. Che, *Talanta*, 1991, **38**(1), 111–114.
7 A. Bratovcic and A. Odobasic, *Determination of Fluoride and Chloride Contents in Drinking Water by Ion Selective Electrode*, InTech, 2011.
8 J. Bujes-Garrido and M. J. Arcos-Martínez, *Talanta*, 2016, **155**, 153–157.
9 J. Bujes-Garrido and M. J. Arcos-Martínez, *Sens. Actuators, B*, 2017, **240**, 224–228.
10 J. Cirello-Egamino and I. D. Brindle, *Analyst*, 1995, **120**, 183–186.
11 J. F. v. Staden and S. I. Tlowana, *Fresenius' J. Anal. Chem.*, 2001, **371**, 396–399.
12 F. Maya, J. M. Estela and V. Cerda, *Talanta*, 2008, **74**, 1534–1538.
13 J. A. Hern, G. K. Rutherford and G. W. Vanloon, *Talanta*, 1983, **30**(9), 677–682.
14 J. A. Morales, L. S. d. Graterol and J. Mesa, *J. Chromatogr., A*, 2000, **884**, 185–190.
15 P. Bruno, M. Caselli, G. d. Gennaro, B. D. Tommaso, G. Lastella and S. Mastrolitti, *J. Chromatogr., A*, 2003, **1003**, 133–141.
16 A. W. Martinez, S. T. Phillips and G. M. Whitesides, *Anal. Chem.*, 2010, **82**, 3–10.
17 A. K. Yetisen, M. S. Akram and C. R. Lowe, *Lab Chip*, 2013, **13**, 2210–2251.
18 M. N. Costa, B. Veigas, J. M. Jacob, D. S. Santos, J. Gomes, P. V. Baptista, R. Martins, J. Inácio and E. Fortunato, *Nanotechnology*, 2014, **25**, 1–12.
19 J. Hu, S. Wang, L. Wang, F. Li, B. Pingguan-Murphy, T. J. Lu and F. Xu, *Biosens. Bioelectron.*, 2014, **54**, 585–597.
20 C. R. Mace and R. N. Deraney, *Microfluid. Nanofluid.*, 2014, **16**, 801–809.
21 P. Tee-ngam, N. Nunant, P. Rattanarat, W. Siangproh and O. Chailapakul, *Sensors*, 2013, **13**, 13039–13053.
22 L. S. A. Busa, S. Mohammadi, M. Maeki, A. Ishida, H. Tani and M. Tokeshi, *Micromachines*, 2016, **7**, 1–21.
23 Y. Chen, G. Fu, Y. Zilberman, W. Ruan, S. K. Ameri, Y. S. Zhang, E. Miller and S. R. Sonkusale, *Food Control*, 2017, **82**, 227e232.
24 B. M. Jayawardane, I. D. McKelvie and S. D. Kolev, *Talanta*, 2012, **100**, 454–460.
25 B. M. Jayawardane, S. Wei, I. D. McKelvie and S. D. Kolev, *Anal. Chem.*, 2014, **86**, 7274–7279.
26 N. A. Meredith, C. Quinn, D. M. Cate, T. H. Reilly, J. Volckens and C. S. Henry, *Analyst*, 2016, **141**, 1874–1887.
27 A. W. Martinez, S. T. Phillips, E. Carrilho, S. W. Thomas, H. Sindi and G. M. Whitesides, *Anal. Chem.*, 2008, **80**, 3699–3707.
28 L. Shen, J. A. Hagenb and I. Papautsky, *Lab Chip*, 2012, **12**, 4240–4243.
29 D. M. Cate, W. Dungchai, J. C. Cunningham, J. Volckens and C. S. Henry, *Lab Chip*, 2013, **13**, 2397–2404.
30 W. Dungchai, Y. Sameenoi, O. Chailapakul, J. Volckensc and C. S. Henry, *Analyst*, 2013, **138**, 6766–6773.
31 K. Yamada, T. G. Henares, K. Suzuki and D. Citterio, *ACS Appl. Mater. Interfaces*, 2015, **7**, 24864–24875.
32 D. M. Cate, S. D. Noblitt, J. Volckens and C. S. Henry, *Lab Chip*, 2015, **15**, 2808–2818.
33 T. Tian, J. Li, Y. Song, L. Zhou, Z. Zhu and C. J. Yang, *Lab Chip*, 2016, **16**, 1139–1151.
34 R. Pratiwia, M. P. Nguyend, S. Ibrahima, N. Yoshiokac, C. S. Henryd and D. H. Tjahjono, *Talanta*, 2017, **174**, 493–499.
35 W. Zhao, M. A. Brook and Y. Li, *ChemBioChem*, 2008, **9**, 2363–2371.
36 G. H. Chen, W. Y. Chen, Y. C. Yen, C. W. Wang, H. T. Chang and C. F. Chen, *Anal. Chem.*, 2014, **86**(14), 6843–6849.
37 N. Ratnarathorn, O. Chailapakul, C. S. Henry and W. Dungchai, *Talanta*, 2012, **99**, 552–557.
38 A. Apilux, W. Siangproh, N. Praphairaksit and O. Chailapakul, *Talanta*, 2012, **97**, 388–394.
39 D. C. M. Ferreira, G. F. Giordano, C. C. de S. P. Soares, J. F. A. de Oliveira, R. K. Mendes, M. H. Piazzetta, A. L. Gobbi and M. B. Cardoso, *Talanta*, 2015, **141**, 188–194.
40 A. Yakoh, P. Rattanarat, W. Siangproh and O. Chailapakul, *Talanta*, 2018, **178**, 134–140.
41 T. Parnklang, C. Lertvachirapaiboon, P. Pienpinijtham, K. Wongravee, C. Thammacharoen and S. Ekgasit, *RSC Adv.*, 2013, **3**, 12886–12894.

Electronic Supplementary Material (ESI) for Analyst.

Supplemental Information

Distance -based Paper Sensor for Determination of Chloride ion Using Silver Nanoparticles

Kamonchanok Phoonsawat[1] • Nalin Ratnarathorn[1]• Charles S. Henry[2] •

Wijitar Dungchai[1]*

1) Organic Synthesis, Electrochemistry & Natural Product Research Unit, Department of Chemistry, Faculty of Science, King Mongkut's University of Technology Thonburi, Prachautid Road, Thungkru, Bangkok, 10140, Thailand

2) Departments of Chemistry and Chemical & Biological Engineering and School of Biomedical Engineering, Colorado State University, Fort Collins, CO 80523.

Corresponding author: Asst. Prof. Dr. Wijitar Dungchai
E-mail: wijitar.dun@kmutt.ac.th
Fax: +66-02-470-8840
Tel: +66-02-470-9553

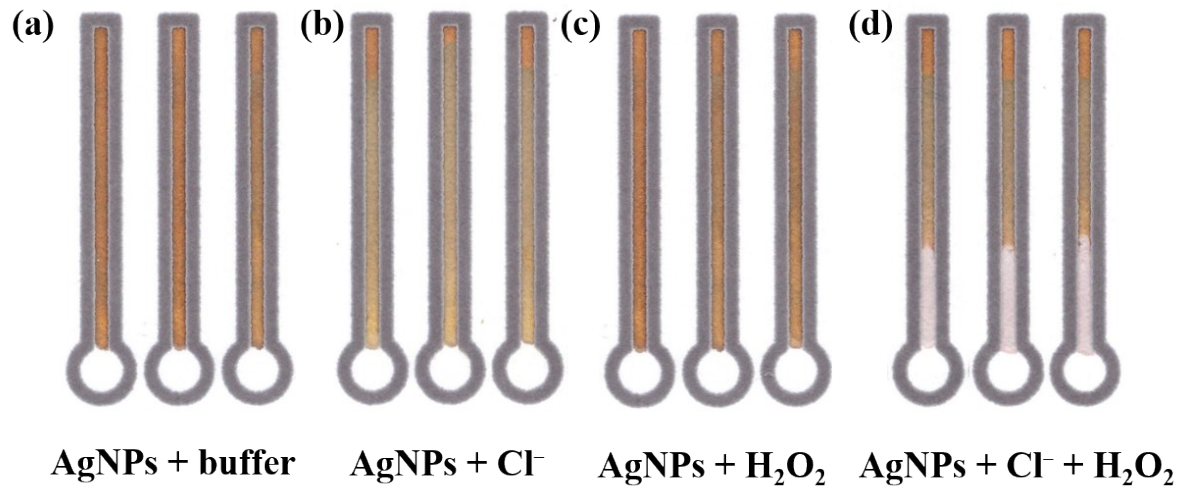

Fig. S1 Paper-based device modified with AgNPs the addition of (a) buffer, (b) Cl^- solution, (c) H_2O_2 solution, and (d) mixture solution of Cl^- and H_2O_2.

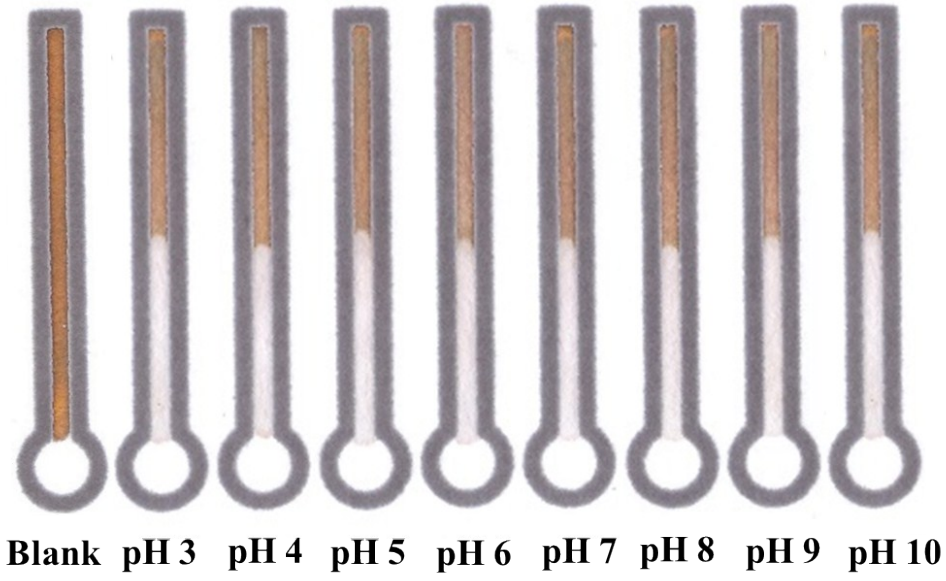

Fig. S2 The effect of pH on the Cl^- determination was determined using a buffer solution in pH range of 3–10.

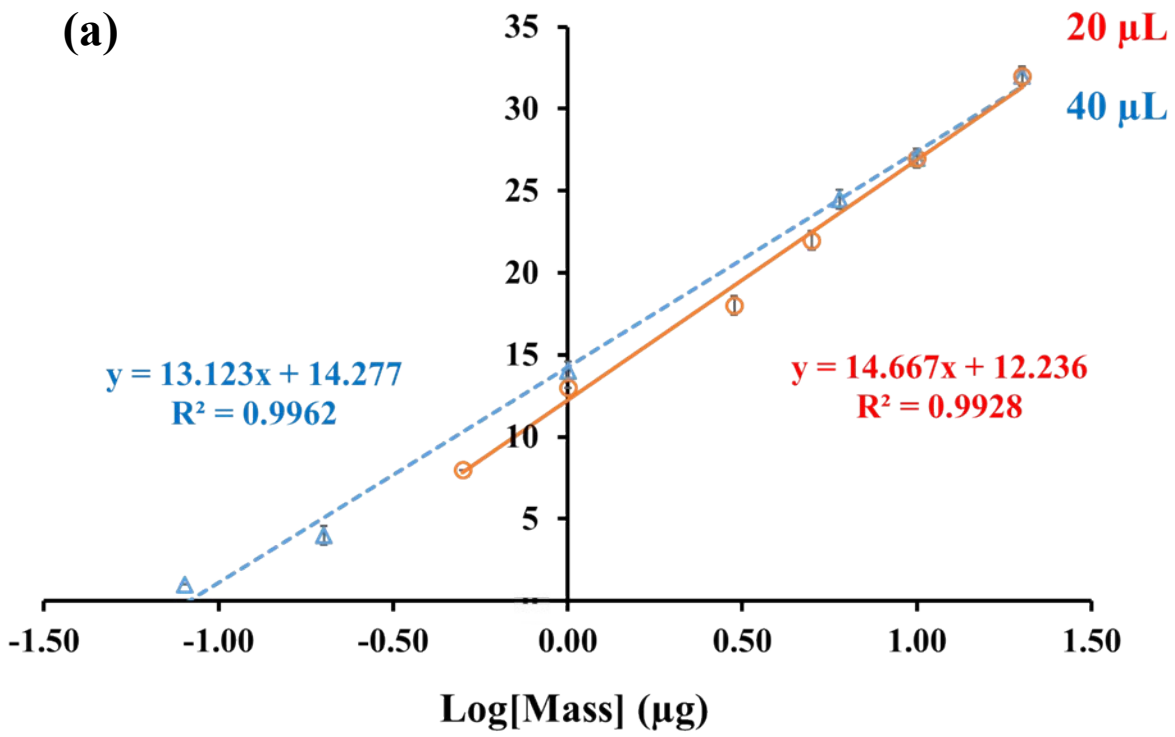

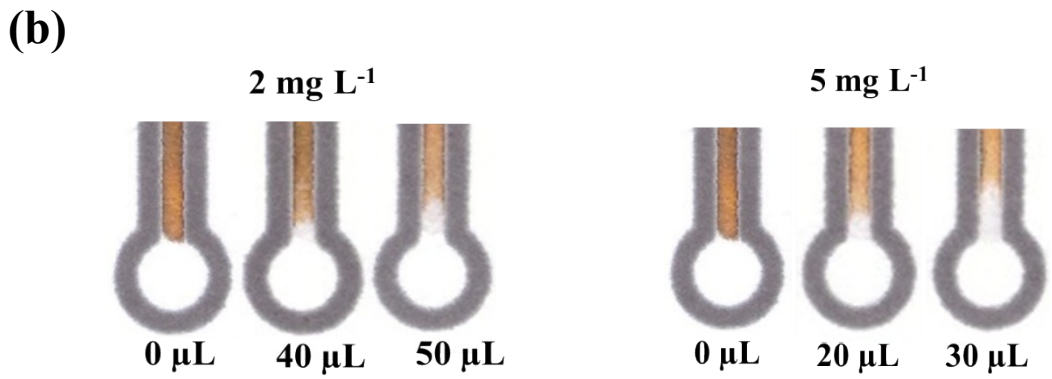

Concentration (2 mg L^{-1})				Concentration (5 mg L^{-1})			
Volume (µL)	0	40	50	**Volume (µL)**	0	20	30
Mass (µg)	0	0.08	0.10	**Mass (µg)**	0	0.10	0.15

Fig. S3 (a) The calibration plot showing the color band distance (*Y*-axis) with the logarithmic mass of Cl^- (*X*-axis) at a volume of sample/standard 20 µL and 40 µL. (b) The mass of 2 mg L^{-1} (volume: 40 µL and 50 µL) and 5 mg L^{-1} of Cl^- (volume: 20 µL and 30 µL)

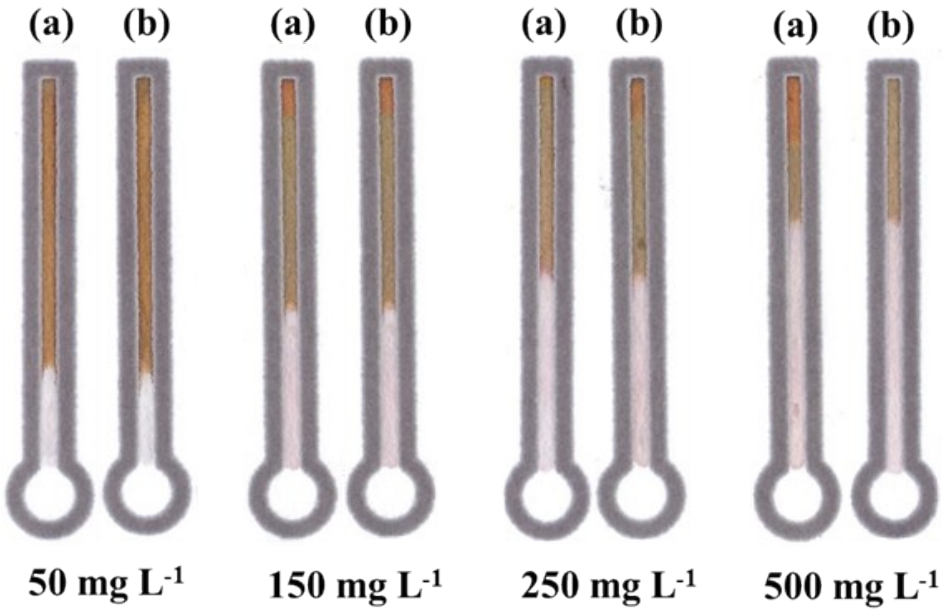

Fig. S4 The color band distance of Cl^- at the sample/standard concentration of 50, 150, 250 and 500 mg L^{-1} is in (a) the ratio of Cl^-: H_2O_2 (1:1) and (b) Cl^-: H_2O_2 (3-4 drops of 0.2%).

Table. S1 Comparison of the percentage of accuracy obtained from our device and test-kit (n = 30).

Sample	%Relative accuracy (n = 30)	
	Our device	Test-kit
Standard 500 mg L^{-1}	91-104%	66-200%
Standard 750 mg L^{-1}	98-105%	100-200%
Standard 1,000 mg L^{-1}	95-102%	50-150%
Standard 1,250 mg L^{-1}	99-106%	40-160%